Molecular Dynamics Simulation of Methanolic and Ethanolic Silica−Based Sol−Gel Solutions at Ambient Temperature and Pressure

ARTICLE *in* THE JOURNAL OF PHYSICAL CHEMISTRY A · JANUARY 2002

Impact Factor: 2.69 · DOI: 10.1021/jp010078h

3 AUTHORS, INCLUDING:

Richard Richard A Catlow
University College London
994 PUBLICATIONS **25,598** CITATIONS

SEE PROFILE

Geoffrey David Price
University College London
268 PUBLICATIONS **7,773** CITATIONS

SEE PROFILE

Molecular Dynamics Simulation of Methanolic and Ethanolic Silica-Based Sol−Gel Solutions at Ambient Temperature and Pressure

J. C. G. Pereira,*,†,‡,§ C. R. A. Catlow,† and G. D. Price‡

The Royal Institution of Great Britain, 21 Albemarle Street, London W1X 4BS, United Kingdom, Department of Geological Sciences, University College London, Gower Street, London WC1E 6BT, United Kingdom, and Materials Engineering Department, Instituto Superior Técnico, Av. Rovisco Pais, 1000 Lisboa, Portugal

Received: January 7, 2001; In Final Form: July 10, 2001

We use molecular dynamics simulations to model realistic silica-based sol−gel solutions containing water, the simplest alcohols (MeOH and EtOH), the simplest silica alkoxides ($Si(OMe)_4$ and $Si(OEt)_4$), and small silica clusters ($Si(OH)_4$, $Si_2O(OH)_6$, and $Si_3O_3(OH)_6$), at ambient conditions. This work builds on our previous studies simulating liquid water, methanol, ethanol, $Si(OMe)_4$, and $Si(OEt)_4$, for different conditions of pressure and temperature.[1] Twelve solutions were simulated during 500 ps, using two different MD codes, DISCOVER and DL_POLY, with slightly different implementations and force fields, to guarantee that the results are not sensitive to details of the simulations. The same methodology is employed throughout to derive potentials for different species, liquid compositions, and thermodynamic conditions. The results obtained with both codes show that silica clusters tend to aggregate, even in dilute solutions, as observed in experimental work—a necessary step before condensation reactions can occur. According to our tests, these results are essentially independent of the initial configuration chosen for the solutions. The solvation environment around the various silica clusters (monomers, dimers and trimer rings) was also investigated, as it gives valuable insight into the diffusional and reaction mechanisms occurring in these solutions.

Introduction

To simulate complex liquid solutions by molecular dynamics or Monte Carlo techniques, we need to develop general methodologies and sets of potentials that work simultaneously for the many different compositions, temperatures, and pressures used in experimental studies. However, many potentials derived for atomistic simulations have been designed to be highly accurate, but system specific. In our previous work,[1] we developed automatic methodologies and potentials that fit the most common properties of liquids with different compositions (water, methanol, ethanol, TMOS (tetramethoxysilane = $Si(OCH_3)_4$), and TEOS (tetraethoxysilane = $O(CH_2CH_3)_4$)), and thermodynamic conditions (high temperature and pressure, ambient conditions).

In this paper we report molecular dynamics simulations of silica-based sol−gel solutions containing molecules of water, alcohols (methanol or ethanol), and alkoxides (TMOS or TEOS), mixed with silica clusters (monomers = $Si(OH)_4$, dimers = $Si_2O(OH)_6$, trimer rings = $Si_3O_3(OH)_6$), at ambient temperature and pressure. We used the approach that had been tested previously for the pure liquids, with varying chemical composition and thermodynamic conditions, to calculate appropriate force fields describing these solutions. This work on sol−gel solutions and the previous work on pure liquids are based on our ab initio studies[2,3] of all silica clusters $Si_xO_y(OH)_z$ with $x \leq 5$, plus water, methanol, ethanol, and TMOS, TEOS molecules.

The present work therefore represents a first attempt to simulate realistic silica-based solutions, using chemical compositions and thermodynamic conditions commonly used in experimental sol−gel research. Special emphasis is given to the following topics: (1) how the improved MD model, presented in our previous article,[1] describes the aggregation of silica clusters and the key interactions that allow the forward and reverse sol−gel reactions to occur; (2) what is the chemical environment around the silica clusters after long simulation times, a central issue in understanding solvation and reaction mechanisms; (3) how MD simulations describe the mixture of the different components in complex liquid solutions and how the final results depend on the initial configuration of the molecules in the simulation box.

Our ultimate goal is to develop a model to simulate the evolution with time of silica-based solutions (containing water, alcohols, silica alkoxides, and a wide range of silica clusters), including the diffusional processes and reaction mechanisms that occur in these systems.

Background. Metal alkoxides, in general, tend to hydrolyze rapidly when exposed to water, according to the reaction

$$M - OR + H_2O \rightarrow M - OH + ROH$$

Transition metal alkoxides are usually too reactive and have to be stabilized by adding complexing agents, such as carboxylic acids or β-diketones, to avoid fast precipitation.[4] Silicon alkoxides are much less sensitive to hydrolysis, due to the high electronegativity of Si, and acid or base catalysis is usually employed in sol−gel processing to enhance their reactivity. Isotopic studies with ^{18}O have shown that the reaction of isotopically labeled water with TEOS produces only unlabeled alcohols in both acid- and base-catalyzed systems,[5] thus

* Corresponding author. Present address: Dept. Eng. Materiais, Instituto Superior Ténico, 1000 Lisboa, Portugal. E-mail: carlos@pehoe.civil.ist.utl.pt. Tel. 351 21 8418111. Fax 351 21 8418132.
† The Royal Institution of Great Britain.
‡ University College London.
§ Instituto Superior Técnico.

10.1021/jp010078h CCC: $22.00
Published on Web 12/11/2001

supporting the hypothesis of a nucleophilic attack of the oxygen of the water molecule on the silicon atom:

$$\mathrm{Si-OR + H_2{}^{18}O \rightarrow Si-{}^{18}OH + ROH}$$

The same behavior is observed in organoalkoxysilanes, $SiR_n(OR)_{4-n}$, with $n = 1$, 2 or 3.[5]

An alkoxide ligand can be exchanged by a different alkoxide ligand, during a transesterification reaction:

$$\mathrm{R'OH + Si(OR)_4 \rightarrow Si(OR)_3OR' + ROH}$$

This reaction has been extensively studied because it is the common method of producing various alkoxides of silicon.[5]

The importance and complexity of the reverse transesterification is shown by the experimental work of Uhlmann et al.[6] When the TEOS hydrolysis is carried out in iPOH, the iPOH concentration initially decreases, due to ester exchange, and then increases toward its original value as hydrolysis proceeds. Furthermore, TEOS hydrolyzes much faster in MeOH than in EtOH, reflecting also ester exchange. However, when TEOS is solvated in MeOH or iPOH, no exchange can be detected, suggesting that the reaction is promoted by and may require the presence of H_2O.

The hydrolysis reaction may proceed in the reverse direction, a reesterification,[5] in which an alcohol molecule displaces a hydroxyl group to produce an alkoxide ligand plus a water molecule:

$$\mathrm{Si-OH + ROH \rightarrow Si-OR + H_2O}$$

The silanol groups formed during the hydrolysis can, in turn, form successive linking disiloxane bonds according to the following water and alcohol condensation reactions, this way leading to the inorganic polymerization occurring in silica-based sol−gel processes:

$$\mathrm{Si-OH + OH-Si \rightarrow Si-O-Si + H_2O}$$

$$\mathrm{Si-OR + OH-Si \rightarrow Si-O-Si + ROH}$$

The reverse process, using water to break SiOSi bonds

$$\mathrm{Si-O-Si + H_2O \rightarrow Si-OH + OH-Si}$$

occurs during the dissolution and deposition of silica in water, involving chemical reactions of hydration:

$$\mathrm{(SiO_2)_n + 2H_2O \rightarrow (SiO_2)_{n-1} + Si(OH)_4}$$

Most alkoxides, in particular TMOS and TEOS, are immiscible with water. A solvent, typically an alcohol, is usually employed to avoid liquid−liquid phase separation. In practice this imposes a higher limit on the amount of water that can be added to the solution for a given alcohol/alkoxide ratio.

The molar ratio of water/alkoxide in solution, R, is a key parameter in silica-based, sol−gel chemistry. As each tetrafunctional precursor, such as TMOS and TEOS, requires four water molecules to be fully hydrolyzed but liberates two during its full condensation, $R = 2$ is enough to complete the sol−gel polymerization in stoichiometric conditions, though $R = 4$ is necessary to allow full hydrolysis to take place before condensation occurs to a significant amount. When the amount of water in solution is low, the rate of hydrolysis should increase rapidly with R, as the interactions between alkoxide and water molecules becomes more probable. For large amounts of water, diffusion constraints should no longer be important and the hydrolysis rate should become almost independent of the concentration of water. The condensation rate should decrease steadily with increasing R, because the interaction between the two silanol groups becomes more difficult and the reverse hydration of the siloxane bonds already formed is favored.

Experimental Studies. A detailed discussion of the hydrolysis and condensation reactions, including precursors, inductive and isotopic effects, pH and solubility, and catalysis can be found in the books by Iler[7] and Brinker et al.,[5] and in the review by Osterholtz et al.[8] Studies regarding temperature and pressure effects, chemical additives, etc. have been reported by Mackenzie,[9] Jonas,[10,11] Orcel et al.,[12,13] and Artaki et al.[14]

Kinetic models to describe the hydrolysis and condensation reactions that occur simultaneously in sol−gel processes have been proposed by Peppas et al. (Branching model[15]), Assink (Functional group model[16]), Re (Bicomponent model,[17] and Kay et al. (nearest-neighbor model[18]).

Experimental work to identify and analyze the silica clusters produced in the first stages of the condensation process have been reported by Kelts et al.,[19] using ^{29}Si NMR spectroscopy, and Klemperer et al.,[20−24] using a combined protocol to separate and measure the clusters: quenching by diazomethane, fractionation using spinning band column distillation, identification by capillary gas chromatography, and structural characterization using ^{29}Si NMR. Knight[25] presents the structures of the 16 so-called secondary building units (SBUs), the common structural subunits used to classify the 64 topologically distinct zeolite networks characterized until 1990 (the primary building units being single SiO_4 tetrahedra). These are compared with the 18 silicate anions determined by ^{29}Si NMR in organic base silicate anions, and the utility of the SBU theory is questioned.

The hydrolysis and condensation reactions are not described in the purely classical simulations carried out in this work, as they imply a further refinement of the whole methodology and force field. Therefore, we prepared ideal solutions that simulate various stages of the sol−gel process: (1) before the hydrolysis reaction occurs, when only water, the alcohol, and the silica alkoxide are present in the solution; (2) after hydrolysis and before condensation, when all molecules of the alkoxide have been hydrolyzed to form silica monomers; (3) after condensation, when all silica monomers have undergone condensation reactions to form silica dimers or (in a subsequent stage) silica trimer rings.

The results obtained for all these systems and conditions are in good agreement with experimental evidence and provide solid support for future full simulations of these important reactive solutions.

Previous Theoretical Studies. The first molecular dynamics simulations related to sol−gel processes were published by Garofalini et al. in 1986[26,27] and consisted of a simulation of the monomer, dimer, and water molecules using a modified Born−Mayer−Huggins (BMH) potential to describe all Si−Si, Si−O, and O−O pairs in the nonwater molecules and a revised Rahman−Stillinger−Lemberg (RSL2) potential to describe all O−H, H−H, and O−O pairs in the water molecules. They found that changing only the BMH potential, both silicic and disilicic acids can be reasonably described and an accurate energy can be obtained for the deprotonation of $Si(OH)_4$ into $SiO_4H_3^-$, in agreement with previous quantum mechanical calculations. Simulations of two silicic acid monomers to describe the condensation reaction were attempted. Although the clusters attracted each other, a water molecule was not formed during the reaction, merely association of the two clusters occurred instead of a true condensation reaction.

Successful simulations of sol−gel condensation reactions were reported by Feuston et al. in 1990[28,29] using only two-

and three-body potentials. The Si−Si, O−O, and O−Si interactions were represented by a modified BMH potential, while Si−H, O−H, and H−H interactions were described by BMH potentials plus additional terms taken from the Rahman−Stillinger−Lemberg potential (RSL2). The O−Si−O, Si−O−Si, H−O−H, and Si−O−H angular distributions were controlled by a combined bond angle−bond length potential. The Si−Si, O−O, Si−O, O−Si−O, and Si−O−Si potentials had been derived previously to simulate vitreous silica[30] and gave a reasonable description of the radial distribution function and structure factor of the glass, in particular by reducing the distribution of tetrahedral angles and the concentration of bond defects to ∼1−2%. The O−O interaction was therefore the same in the water and silica subsystems. For temperatures above 1500 K, this model is able to simulate the onset of polymerization, leading to the formation of oligomers as large as six-silicon chains in less than 20 ps. An OH group is first deprotonated, leaving a negatively charged $Si-O^-$ group, which subsequently attacks another monomer, forming a unstable pentaccordinated silicon that finally relaxes by the dissociation of a OH^- group.

This empirical model was studied later[31] for longer run times, of about 120 ps, showing that the chains formed during the early stages of the simulation can close to form rings with 3 to at least 8 silicon atoms. The activation energy for formation of branching Q_m^n species (12 kcal/mol) is consistent with the experimental data of 12 kcal/mol for gelation and compares well with the activation enthalpy of condensation between two monomers, found experimentally,[31] of 15 kcal/mol. Other studies included the analysis of molecular mechanisms and the effect of hydrogen in sol−gel polymerization.[32] Molecular dynamics simulations of silica aerogels have been reported by Pohl et al.[33] Three different modeling methods are presented, and the results obtained are compared with experimental data derived from small-angle X-ray scattering, nuclear magnetic resonance, and gas adsorption.

The modeling of glass systems (since the first MD simulation of glass formation carried out by Woodcock in 1971, who cooled molten KCl) is discussed in the 1982 review of glass structure and diffusion in glass published by Soules.[34] Later MD simulations of silica-based glasses include the work of Vessal et al.,[35] proposing three different potential models to describe vitreous silica, Newel et al.,[36] Zirl et al.,[37] and Melman et al.,[38] developing models to simulate sodium trisilicate and sodium aluminosilicate glasses. Ab initio studies of silica clusters using both Hartree−Fock and functional density levels of theory, have been reported by Lasaga et al.,[39,40] Sauer,[41] Ahlrichs et al.,[42] Ferrari et al.,[43] Pápai et al.,[44] Hill et al.,[45] and Moravetski et al.[46] for clusters as large as the sodalite cage, with 24 silicon atoms. Ab initio interatomic potentials proposed by Tsuneyuki for silicon dioxide have been tested for α-quartz under pressure, by Chelikowsky et al.[47] Molecular dynamics simulations of SiO_2 melt and glass have been carried out by Kubicki et al.[48] using two sets of ionic and covalent interatomic potentials. Monte Carlo simulations of amorphous silicon have been done by Dereli[49] using two-body and three-body Stillinger−Weber potentials (the potentials are fully described).

Simulation of solvation and mixing effects in liquids attracted progressively more attention in the second half of the 1980s. Fleischman et al. used molecular dynamics coupled with thermodynamic cycle perturbation theory[50] to calculate relative Helmholtz free energies of hydration for methanol, ethanol, ethane, and propane. Equimolar mixtures of methanol and water were studied by Stouten et al.[51] using NPT molecular dynamics, following previous simulations of liquid water and methanol. They concluded that both the volume contraction and the excess enthalpy of the solution can be well described with the SPC and OM2 potentials developed for pure water and methanol. These results support the assumption that sol−gel solutions can be simulated with the methodologies and potentials developed for pure liquids.

The effect of different initial sites for water molecules in crystal hydrates has been studied by Howell et al.,[52] comparing MC simulations started from random and experimental configurations. It was found that the overall hydrogen-bond structure could be reproduced in both cases, but some differences still persist after 600 000 configurations.

The effect of the molecular separation of the reacting species on the polycondensation of $Si(OCH_2CH_3)_4$ was studied by Yoldas[53] using a combination of size-excluded liquid chromatography (SEC) and ^{29}Si NMR. It was shown that the mean value and distribution of the molecular weight of the resultant organosiloxane polymers depends considerably on the molecular separation between the reacting TEOS molecules in the initial solution. The molecular structure and molecular size distribution in sol−gel processes are thus determined primarily by chemical encounter rates and the diffusion process.

The Present Work. In the present study, we used two different MD codes: DISCOVER from Molecular Simulations Inc.[54] and DL_POLY from the Daresbury Laboratories,[55] with slightly different implementations and force fields, to analyze how these theoretical differences influence the results and to guarantee that our main conclusions are essentially independent of the code implementation.

Two compositions were studied with the DISCOVER code in this work: the first with 200 water molecules and 200 methanol molecules plus 8 monomers $Si(OH)_4$, and the second with 200 water molecules and 200 ethanol molecules plus 8 trimer rings $Si_3O_3(OH)_6$ (approximately 0.5 mol/L of $Si(OH)_4$). Methanol and ethanol were chosen because they are the most commonly used solvents in sol−gel processes. For each composition, three initial configurations were considered (resulting thus in a total of six solutions): one with all the water molecules on one side and the alcohol molecules on the other; a second with water and alcohol molecules occupying alternate octant cubes of the cell; and finally a third with all water and alcohol molecules with alternating positions in the initial configurations. The silica clusters are uniformly distributed in all configurations. Large trimer rings were chosen to decrease diffusion and make the test of the mixing conditions more stringent. Highly dilute solutions were chosen to make the test of the aggregation conditions more stringent. (These compositions would correspond to initial solutions with ratios water/TMOS = 29 and methanol/TMOS = 21 for the methanolic solutions, and water/TEOS = 11.3 and ethanol/TEOS = 4.3 for the ethanolic solutions.)

Three ideal stages of the sol−gel process were investigated with the DL_POLY code for real sol−gel solutions with composition water/alkoxide = 4 and alcohol/alkoxide = 8: first, before the hydrolysis, with 30 molecules of alkoxide ($Si(OR)_4$) plus 120 molecules of water plus 240 molecules of alcohol; second, after the full hydrolysis but before the condensation, with 30 molecules of monosilicic acid ($Si(OH)_4$) plus 360 molecules of alcohol; and third, after the first stage of condensation, with 15 molecules of disilicic acid ($Si_2O(OH)_6$) plus 15 molecules of water and 360 molecules of alcohol. Two sets of solutions were investigated, one containing methanol and TMOS ($Si(OCH_3)_4$), the other containing ethanol and TEOS ($Si(OCH_2CH_3)_4$), resulting in a total of six sol−gel solutions.

Computational Details

Simulations with DISCOVER 2.9. We used a cubic cell with a minimum image convention, a group-based method, and a 9 Å cutoff for all Coulombic and van der Waals long-range interactions (i.e., no Ewald sum). The equations of motion were integrated with a Verlet leapfrog algorithm using a 1 fs (10^{-15} s) time step, and the NPT conditions were simulated by a Berendsen algorithm using 1 and 50 fs for temperature and pressure relaxation times. A smaller time step, 0.5 fs, was used in the ethanolic solutions, due to some instability created by the large trimer rings.

The ab initio 9−6−1 cff91 force field developed by Molecular Simulations Inc.,[54] containing quartic bond length and quartic bond angle terms, a three Fourier term for dihedral angles, and cross terms between the various bond terms, was used in all simulations using the DISCOVER code. The parameters derived for zeolites published by Hill et al.[45] (and obtained from Hartree−Fock ab initio calculations) were used in the silica clusters. The bond lengths and bond angles for the Si−O−C potentials, not included in the cff91 and silica force fields, were obtained from our previous density functional ab initio calculations using the DMOL code,[2,3] while the force constants were obtained from geometric averages of the Si−O−Si and C−O−C similar interactions. The partial charges for all atoms were obtained by multiplying by 2.6 the Hirshfeld charges calculated with DMOL for each optimized individual molecule. As reported in our previous article,[1] this factor was found to represent the best compromise to reproduce the experimental data available for the pure liquids that we studied.

To avoid overlaps between the molecules and to allow them to move freely to equilibrium positions, all solutions were initialized disposing the molecules first along cubic lattice positions inside a cubic cell with a low density of ca. 0.25 g/cm^{-3}. After an initial NVT run (at a low temperature) of 10 ps to eliminate intramolecular residual tensions, all simulations were prepared compressing first at 10 000 atm during 10 ps before relaxing to ambient conditions during 20 ps. Successive configurations were then collected every 100 ps until completing 500 ps. G_{SiSi} RDFs were measured for these configurations, which then ran for more 10 ps, to collect the density and energetic data. Instantaneous radial distribution functions were collected during 10 time steps of 0.001 fs each.

Simulations with DL_POLY 1.1. As before, we used a cubic cell with PBC conditions, a minimum image convention, a Verlet leapfrog integration algorithm, and a Berendsen NPT ensemble. An Ewald sum with $\alpha = 0.30$ and $q_{max} = 6$ was used to calculate the long-range Coulombic interactions for all systems and thermodynamic conditions. Contributions for energy and pressure due to the van der Waals interactions that are longer than the real space cutoff were estimated using long-range corrections, as described by Allen and Tildesley.[56] Improvements over the previous DISCOVER simulations included an atom-based method to calculate interactions and a larger cutoff of 11.0 Å for the real space contributions. A time step of 0.5 fs was used for all six solutions.

As before, the 9−6−1 cff91 force field developed by Molecular Simulations Inc.,[54] the silica potentials,[45] and our Si−O−C parameters[1] were used in all DL_POLY simulations, but the cross terms were not applied. Not only is the influence of these terms small and their accuracy questionable, but they make calculations more complex and slower. However, they might be important in calculations of vibrational properties, which are not considered in this work. As discussed in our previous article,[1] to fit the experimental data, the atomic Coulombic charges were obtained by multiplying by 2.7 (instead of 2.6, used with DISCOVER) the Hirshfeld atomic charges of each molecule optimized in our earlier ab initio DFT studies.[2,3] As reported in our previous article,[1] this force field was exhaustively tested against experimental data (density, enthalpy of vaporization, radial distribution functions, self-diffusion coefficients) for high temperature, high pressure, and ambient conditions for liquid water, heavy water, methanol, ethanol, TMOS, and TEOS, where experimental data to compare is widely available.

The low-density initial configurations were compressed first to 10 000 atm and 20 °C for 20 000 time steps (10 ps), and then relaxed for ambient conditions, at 1 atm and 20 °C for another 20 ps to equilibrate the solutions. After this initial procedure, the configurations of the six solutions were collected for analysis after every 50 ps until reaching a run time of 500 ps.

Densities and energies are presented for every 50 ps configuration after 1 ps of collecting time. Densities, energies, and key radial distribution functions for forward and reverse reactions are presented for 100, 300, and 500 ps MD run times, after 5 ps of collecting time. The aggregation of the silicate clusters and the chemical environment surrounding each silicate cluster are analyzed for the same run times by visual inspection of the solutions.

As usual, in both DL_POLY and DISCOVER simulations, scaling factors for intramolecular nonbond energies were made equal to 0.0 for 1−3 interactions and 1.0 for 1−4 interactions (1−*n* interactions occur between atoms in chain positions 1 and *n*; adjacent atoms have 1−2 interactions). Both DISCOVER and DL_POLY simulations were implemented using a fully atomistic force field, obtained entirely from ab initio calculations. Technical details and further references to all the methods mentioned here can be found elsewhere.[56] A detailed description of the force field used in all DISCOVER and DL_POLY simulations is presented in the appendix.

Results

We now report the results obtained for the six solutions simulated with DL_POLY and the six solutions simulated with DISCOVER, covering the following topics: (1) pair interactions promoting forward and reverse reactions; (2) aggregation effects between the various silica clusters; (3) mixing effects regarding solutions with different initial configurations; (4) time evolution of energy and density observed for all solutions; (5) solvation effects regarding the local environment seen by the different silica clusters at the end of the simulations. We will focus more on the results obtained with the DL_POLY code, using a slightly better level of theory.

Reactive Interactions with DL_POLY. A chemical reaction in solution is a three-stage process: (1) the diffusion of the reactants to each other; (2) the replacement of reactant−solvent by reactant−reactant interactions; (3) the chemical transformation itself, when the orientation and energy of the reactants is adequate. The first stage depends essentially on the concentration of the solution, on the size of the reactant molecules, and on the strength of the reactant-solvent interactions; the second stage depends mainly on the relative strength of the concurrent reactant−solvent and reactant−reactant interactions.

To study these nonreactive aggregation steps, the liquid structure should be investigated as a function of time. In sol−gel processes, where the analysis is made more difficult by the large number of reactions and species involved, the simulation of ideal solutions (representing ideal stages of the reaction

process) simplifies considerably the task, focusing on its essential aspects.

The first two solutions studied here, containing 30 molecules of alkoxide (TMOS or TEOS), 120 molecules of water and 240 molecules of alcohol (MeOH or EtOH, respectively), emulate realistic sol−gel solutions before the hydrolysis reaction starts. HCl was not added to the solutions because, even for pH = 1, the corresponding 10^{-1} M concentration of H^+ corresponds to only 2.6 ions per cell. Because the reactions are actually not simulated, acid catalysis effects in solution cannot be studied yet. In these conditions, the only possible reaction is the hydrolysis of the alkoxides, replacing an alkoxyl by an hydroxyl group:

$$Si(OR)_4 + H_2O \rightarrow Si(OR)_3OH + ROH$$

The reverse reaction can then occur, replacing an hydroxyl by an alkoxy group—a reesterification. In principle, these reactions are promoted by O(water) → Si(alkoxide) and O(alcohol) → Si(alkoxide) nucleophilic attacks. The radial distribution functions for these key interactions, as a function of time, are presented in Figure 1 for methanol- and ethanol-based solutions, respectively. Strictly speaking, the O(alcohol)−Si(alkoxide) interaction calculated here describes the transesterification reaction, the replacement of an alkoxy group OR by another OR′. Since the Si environment remains almost the same after removing the first OR group, that interaction describes also the reesterification.

Clearly, the peak for the O(water)−Si interaction, favoring the forward reaction, is much stronger than the peak for the O(alcohol)−Si interaction, favoring the reverse process. Although there are, in solution, twice as many molecules of alcohol than molecules of water, these latter are much smaller and have larger oxygen charges, which tends to result in them avoiding the outer alkyl groups and approaching closer to the inner silicons, with large positive charges. As the comparison of the results for methanolic and ethanolic solutions shows, larger alkyl groups in alkoxides and alcohols increase the O(water)−Si and decrease the O(alcohol)−Si interactions. As can be seen for both solutions, time also favors the forward reaction. The O(alcohol)−Si interactions are relatively stable; there is an increase of the O(water)−Si first peak (around 4 Å), accompanied by a decrease of the second peak (around 6 Å).

The shortest intermolecular Si−O lengths predicted by the 9−6−1 interatomic potentials used in these simulations are in the range 3.0−4.0 Å. To describe shorter distances, ab initio studies are required to develop potentials that can accurately describe the reaction mechanisms and electronic structure changes. Our previous studies[57] of the condensation reaction between a monomer and a protonated monomer, to give a protonated dimer plus a water molecule (acid conditions), using DFT and the COSMO solvation model allowed us to describe different reaction mechanisms with step increments of only 0.2 Å from the reactants to the products, including energy, geometry, and electronic structure.

The next two solutions, containing 360 molecules of alcohol (MeOH or EtOH) and 30 molecules of monosilicic acid, would be generated from the first by the completion of the hydrolysis reaction:

$$30Si(OR)_4 + 120H_2O + 240ROH \rightarrow 30Si(OH)_4 + 360ROH$$

In these solutions two reactions can occur: the forward condensation reaction, replacing two hydroxyl groups by a disiloxane bond

$$Si(OH)_4 + Si(OH)_4 \rightarrow Si_2O(OH)_6 + H_2O$$

and the reverse reesterification

$$Si(OH)_4 + ROH \rightarrow Si(OH)_3OR + H_2O$$

Assuming again that both reactions are promoted by nucleophilic O(monomer) → Si(monomer) and O(alcohol) → Si(monomer) attacks, the corresponding RDFs for these interactions are presented in Figure 2 for methanol- and ethanol-based solutions.

In both cases, the O(monomer)-Si interaction becomes stronger for longer times, while the O(alcohol)-Si interaction remains stable in the methanolic and decreases in the ethanolic solution (due to the larger alkyl groups). In both solutions, after 300 ps, the O(monomer)−Si interactions, favoring the forward condensation reaction, become much stronger than the O(alcohol)−Si interactions, promoting the reverse reesterification. This result is particularly impressive taking into account that there are 360 alcohol molecules in solution and only 30 monomers. Clearly, the monomers are much more attracted to each other than to the solvent, methanol, or ethanol. While in the previous solutions the first peak, representing the O−Si interactions between the alkoxides, starts at 3.2 Å, with the monomers it starts rising at 3.0 Å or even less, as in O(monomer)−Si interactions.

The last two solutions, containing 360 molecules of alcohol (MeOH or EtOH) and 15 molecules of disilicic acid, may be generated from the second sets by completion of a reaction in which all monomers form dimers, by a water condensation reaction:

$$30Si(OH)_4 + 360ROH \rightarrow 15Si_2O(OH)_6 + 15H_2O + 360ROH$$

Four different reactions can be considered in these solutions. First is the forward condensation:

$$2Si_2O(OH)_6 \rightarrow Si_4O_2(OH)_{12} + H_2O$$

second the reverse reesterification:

$$Si_2O(OH)_6 + ROH \rightarrow Si_2O(OH)_5OR + H_2O$$

third the reverse hydrolysis:

$$Si_2O(OH)_6 + H_2O \rightarrow 2Si(OH)_4$$

and fourth the reverse alcoholysis:

$$Si_2O(OH)_6 + ROH \rightarrow Si(OH)_4 + Si(OH)_3OR$$

Assuming, as before, that all reactions start with a O → Si nucleophilic attack, the corresponding key interactions O_t(dimer) → Si, O(alcohol) → Si, and O(water) → Si are analyzed in Figure 3 for methanol- and ethanol-based solutions.

In both cases, the O(dimer)−Si interactions increase considerably with time and the O(water)−Si interactions drop substantially. The O(alcohol)−Si interactions decrease also in the methanolic solution but remain stable in the ethanolic solution. In both solutions, after 500 ps, the O(dimer)−Si interaction, favoring the forward condensation reaction, is already more important than the other two that promote the reverse reactions. Again, these results are even more convincing when taking into

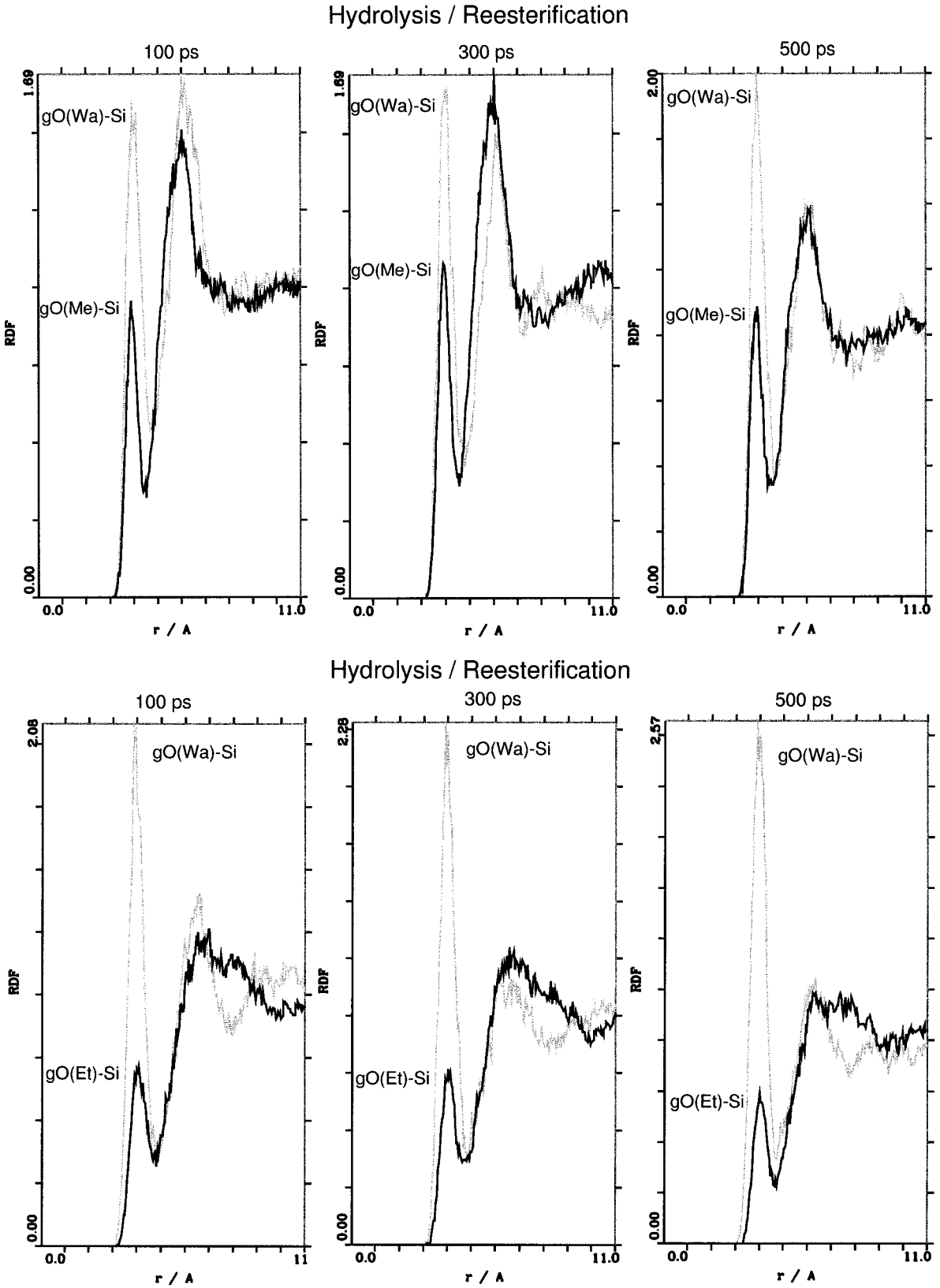

Figure 1. O(water)−Si(alkoxide) and O(alcohol)−Si(alkoxide) pair distributions after DL_POLY simulations in methanolic (above) and ethanolic (below) solutions before hydrolysis, for 100, 300, and 500 ps of run time and 5 ps of collecting time.

account that there are only 15 dimers in solution, against 360 alcohol molecules. There are also only 15 water molecules, but their small size and higher charges should help the O(water)−Si interactions.

Aggregation Effects with DL_POLY. An important aggregation effect is observed in these solutions between both the monomers and the dimers. This aggregation of the silica clusters in solution can indeed be seen, by visual inspection of the final configurations of the six solutions, conveniently stripped of the water and alcohol molecules as represented in Figure 4. Clearly, relatively dense clouds of monomers can be seen in several parts of the cell. This effect is particularly visible taking into account

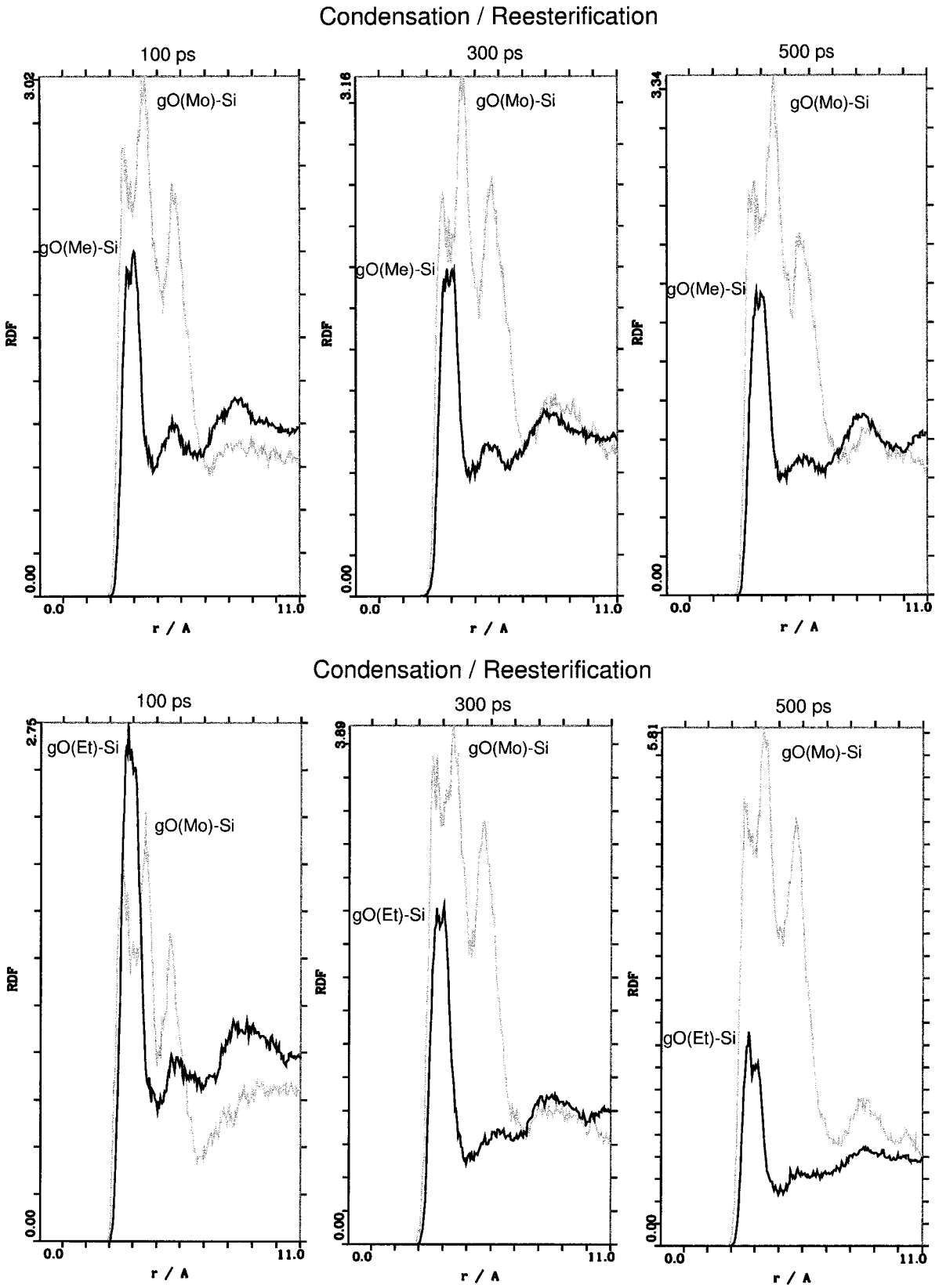

Figure 2. O(monomer)−Si(monomer) and O(alcohol)−Si(monomer) pair distributions after DL_POLY simulations in methanolic (above) and ethanolic (below) solutions after hydrolysis but before condensation, for 100, 300, and 500 ps of run time and 5 ps of collecting time.

the periodic boundary conditions of the system, so molecules in opposite sides of the cell are actually interacting directly with each other.

The dimer aggregation is even more evident, with large regions of the space completely empty of silica clusters, which are concentrated in just a small number of regions across the cell.

Aggregation effects between the alkoxides are difficult to display due to the numerous alkyl groups present, which render the image too complex. These alkyl groups, which are relatively

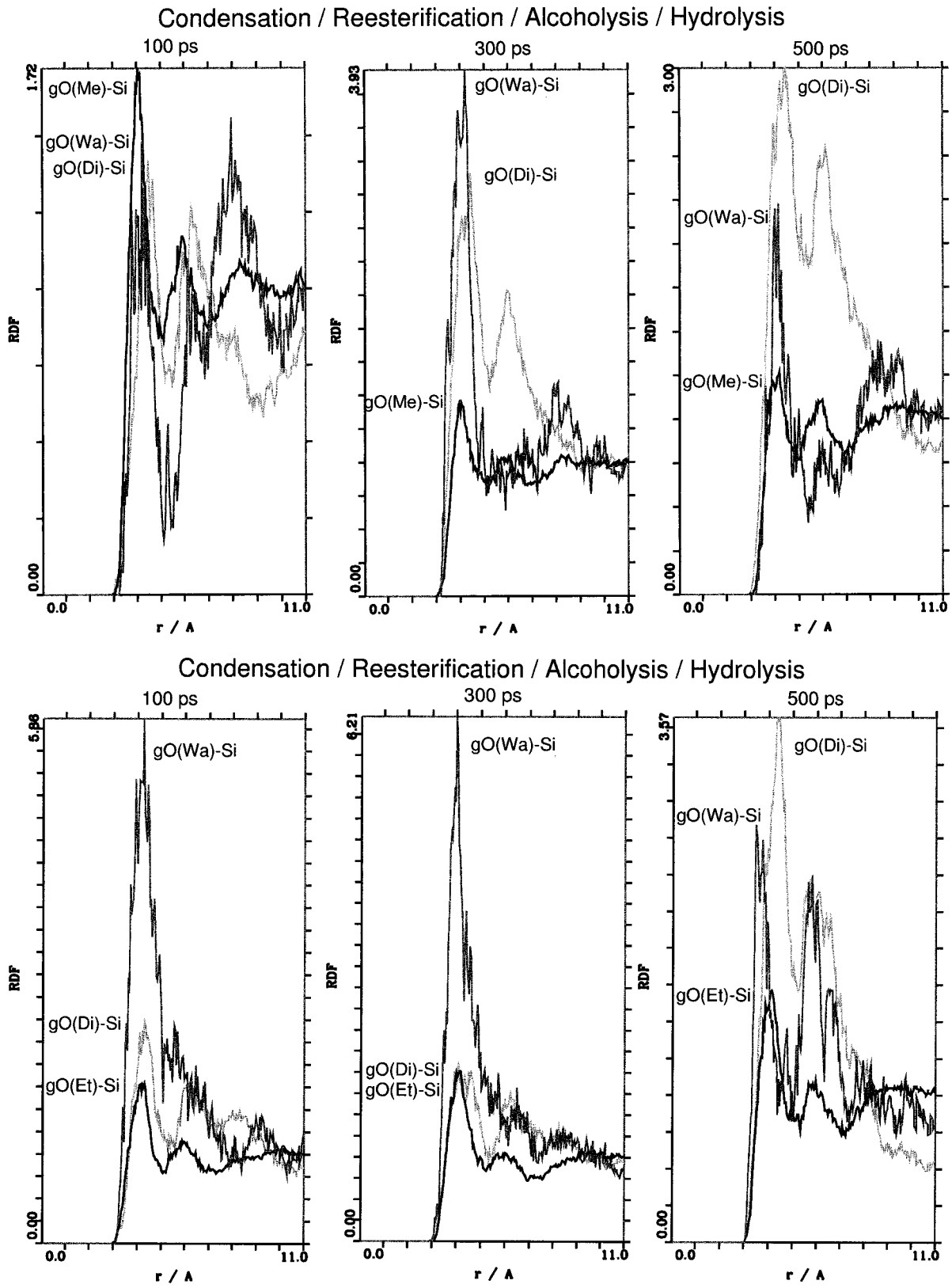

Figure 3. O(dimer)−Si(dimer), O(water)−Si(dimer), and O(alcohol)−Si(dimer) pair distributions after DL_POLY simulations in methanolic (above) and ethanolic (below) solutions after condensation for 100, 300, and 500 ps of run time and 5 ps of collecting time.

large and with small positive charges on all the outer hydrogens, will make O(alkoxide)−Si interactions energetically unfavorable. Although such interactions are not particularly important in sol−gel processes, because no chemical reaction is involved, they may give an indication of the difficulty of a monohydrolyzed alkoxide in attacking another alkoxide in a alcohol-forming condensation:

$$Si(OR)_3(OH) + Si(OR)_4 \rightarrow Si_2O(OR)_6 + ROH$$

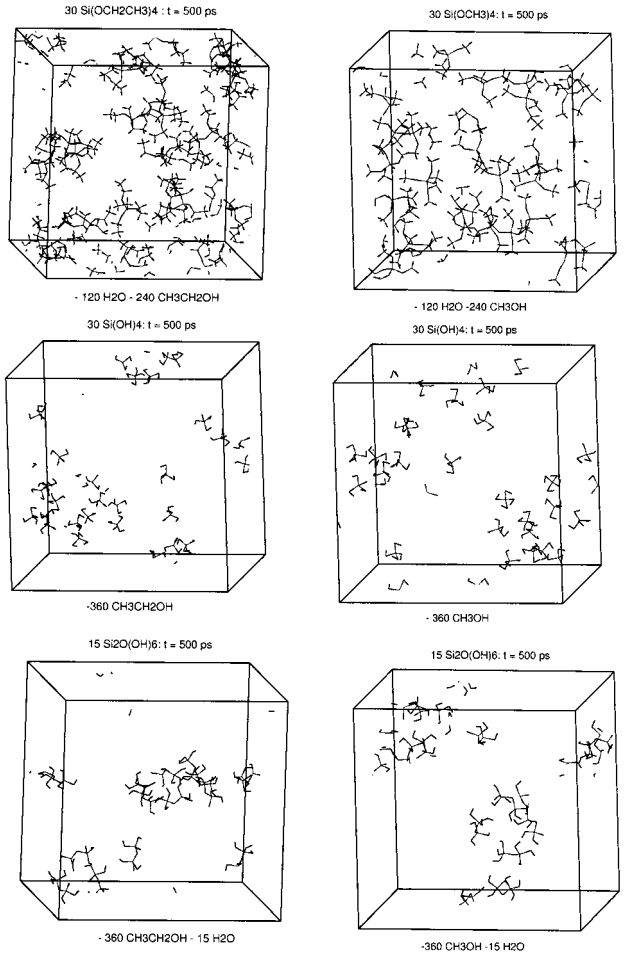

Figure 4. Methanolic (right) and ethanolic (left) solutions after DL_POLY simulations before hydrolysis, after hydrolysis but before condensation, and after condensation, showing only the alkoxide, monomer, and dimer molecules, after 500 ps of run time.

A quantitative description of the aggregation of the silicate clusters is given by the Si−Si radial distribution functions as a function of time, presented in Figure 5 for all six solutions.

In both alkoxide solutions, the Si−Si first peak is relatively weak, does not show any increase with time, and occurs at relatively large distances: 6.5 Å (methanol-based) to 7.5 Å (ethanol-based). However, these distances are exactly the same as in liquid TMOS and TEOS, respectively, at ambient pressure and temperature[1] and show that aggregation is actually occurring, though intermolecular Si−Si interactions remain distant due to the bulky alkoxy groups.

In contrast, the monomer−monomer aggregation is demonstrated by the steady increase, with time, of the first Si−Si peak in both methanolic and ethanolic solutions.

The Si−Si RDF analysis for the dimers is less clear, partially because the statistical weight is now considerably smaller, 15 instead of 30, and because these are two-center molecules, so the relative orientation of the interacting dimers can interfere with the results. Nevertheless, the dimer aggregation is still visible, as the Si−Si first peak is much higher for 500 ps than for 100 or 300 ps, in the ethanolic solution and is much higher for 300 and 500 ps than for 100 ps in the methanolic solution.

Initially the alkoxide molecules attract each other but the Si atoms remain far apart, separated by the alkoxy groups. When alkoxy are replaced by hydroxyl groups, aggregation becomes more important and intermolecular Si−Si distances decrease considerably, making possible the subsequent condensation reaction. We interpret these aggregation effects as due to the larger (silicon and oxygen) charges of the silica clusters, when compared with water and alcohol molecules, resulting in stronger Coulombic interactions that tend to attract the silica clusters together.

Aggregation Effects with DISCOVER. The analysis of the instantaneous Si−Si radial distribution functions, presented in Figures 6 and 7, shows that during the MD simulation the silica clusters tend to approach each other, with the first Si−Si peaks becoming progressively more important and shifted to smaller distances, until a minimum of 4.5 Å. As the cell length in methanolic and ethanolic solutions is about 28 and 31 Å, respectively, the distance between the monomers and between the rings would be about 14 and 15.5 Å if the silica clusters were completely dispersed, corresponding in both cases to 14 Å between the silicon atoms. Although Si−Si first peaks between 14 Å and, say, 8 Å might result only from the thermal Brownian motions inside the solutions, the much smaller Si−Si distances observed in all solutions studied show that, in fact, the silica clusters are aggregating.

The effect mentioned above is also observed by visual inspection of the six final solutions after removing the water and alcohol molecules, as shown in Figure 8. The interaction of the silica clusters seems to be even more important for the larger trimer rings than for the monomers, probably due to the larger scattering cross section of the rings and the larger charge of the ring silicon atoms.

These results confirm entirely the RDF analysis and visual observations obtained with DL_POLY (discussed above) and show that the aggregation effects occurring in sol−gel solutions (and required for condensation reactions to occur) can be simulated by molecular dynamics techniques.

Mixture Effects with DISCOVER. It is important to study the mixture of various species with molecular dynamics for two reasons. First, it is necessary to guarantee that the results obtained for MD simulations of relatively complex sol−gel solutions are independent of the initial configuration chosen, which only happens if the mixture of the various components occurs effectively in a reasonable amount of time, after which no bias or signal of the initial configuration can be observed. The second reason is more physical. The first step in any sol−gel process is always the mixture of its constituents, and, consequently, a realistic simulation should be able to describe the mixture of completely separated components to form a homogeneous solution.

The initial configurations of the six solutions, containing water, an alcohol, and a silicate cluster, specifically designed to study mixture and aggregation effects in sol−gel processes, are presented in Figure 9. The MD solutions for which the formation of a mixture should be more difficult, i.e., the two initially unmixed (one containing water, methanol, and monomers and the other, water, ethanol, and trimer rings) are illustrated in Figures 10 and 11 after 500 ps of simulation. To make the analysis easier, the molecules are shown without using the periodic boundary conditions to generate their replicas inside the cell.

These figures show that the mixture of alcohol and water seems to be completed and neither of the two solutions shows signals of their initial unmixed condition. This evidence is particularly remarkable for the ethanolic solution, where the diffusion and mixture mechanisms should be slower due to the larger size of the ethanol and trimer ring molecules. These results, which were also obtained for the other four solutions

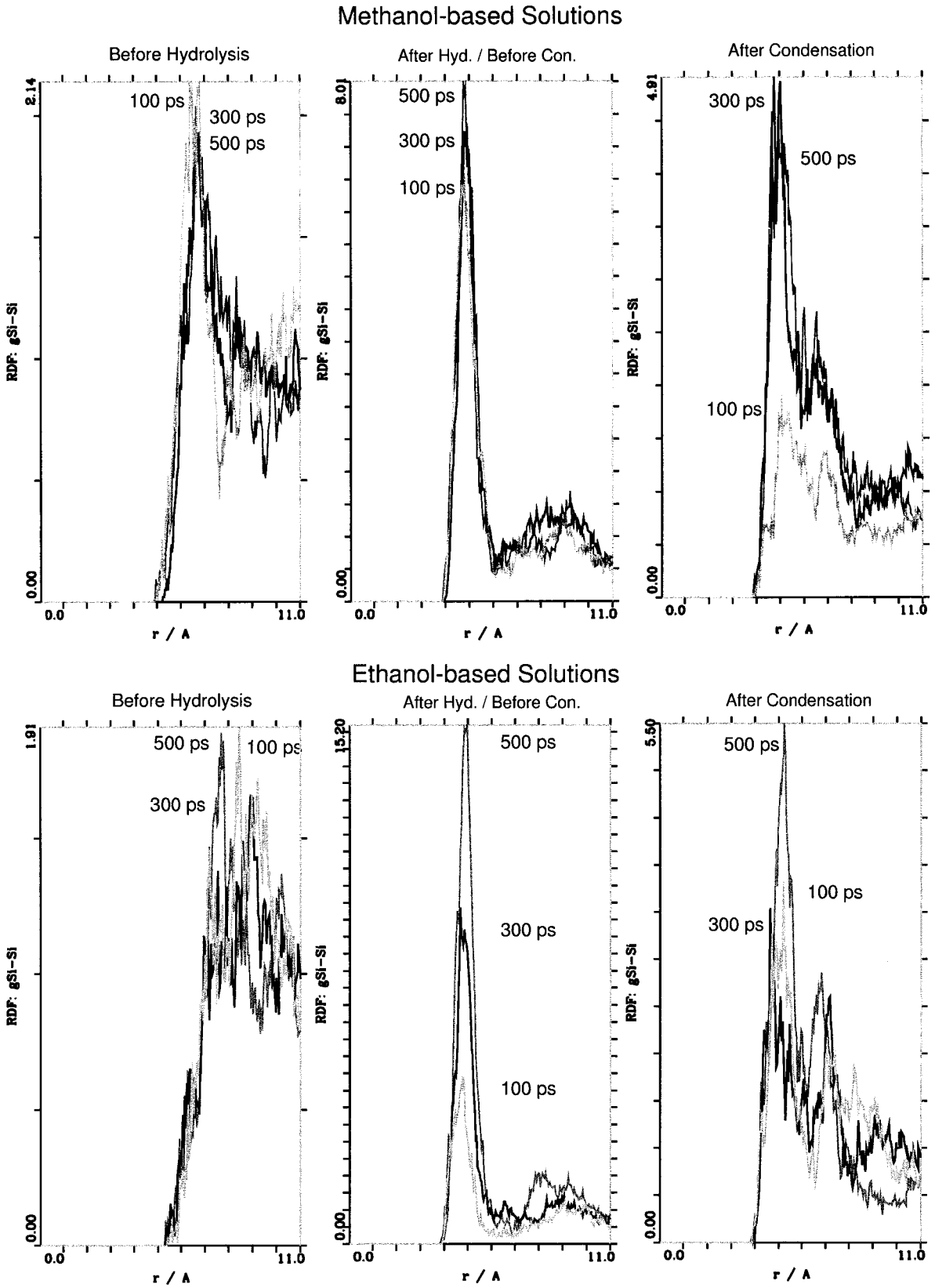

Figure 5. Si−Si pair distributions, in methanolic and ethanolic solutions after DL_POLY simulations, before hydrolysis, after hydrolysis but before condensation, and after condensation, for 500 ps of run time and 5 ps of collecting time.

that were initially mixed or partially mixed, should be a consequence only of the potentials used and therefore should remain valid in more sophisticated MD or MC simulations.

This visual analysis is confirmed by the instantaneous Si−Si intermolecular radial distribution functions calculated for the same solutions and times presented in Figures 6 and 7. Instantaneous RDFs were chosen for this study, instead of averages over time, as the structure of the solutions change progressively with time due to the mixture of the various components.

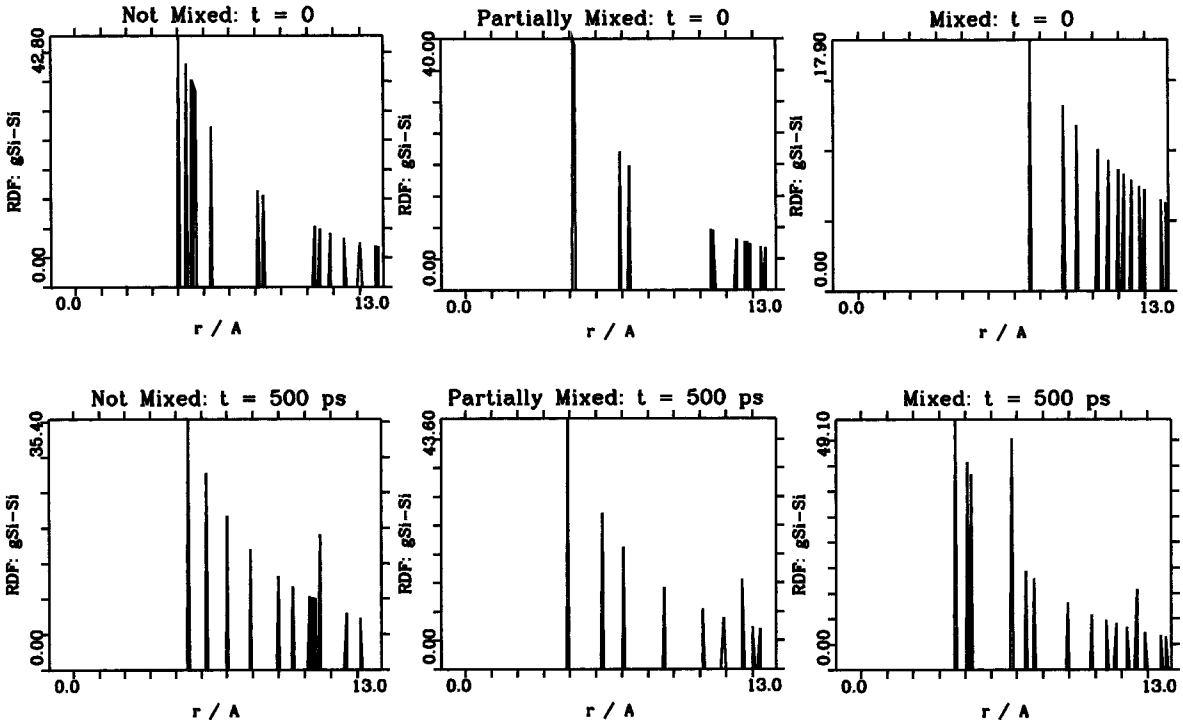

Figure 6. Instantaneous Si−Si pair distributions between monomers after DISCOVER simulations, in methanolic solutions, initially mixed, partially mixed, and unmixed, after 500 ps of run time. The density (g/cm^3) and cell length (Å) are indicated for each solution.

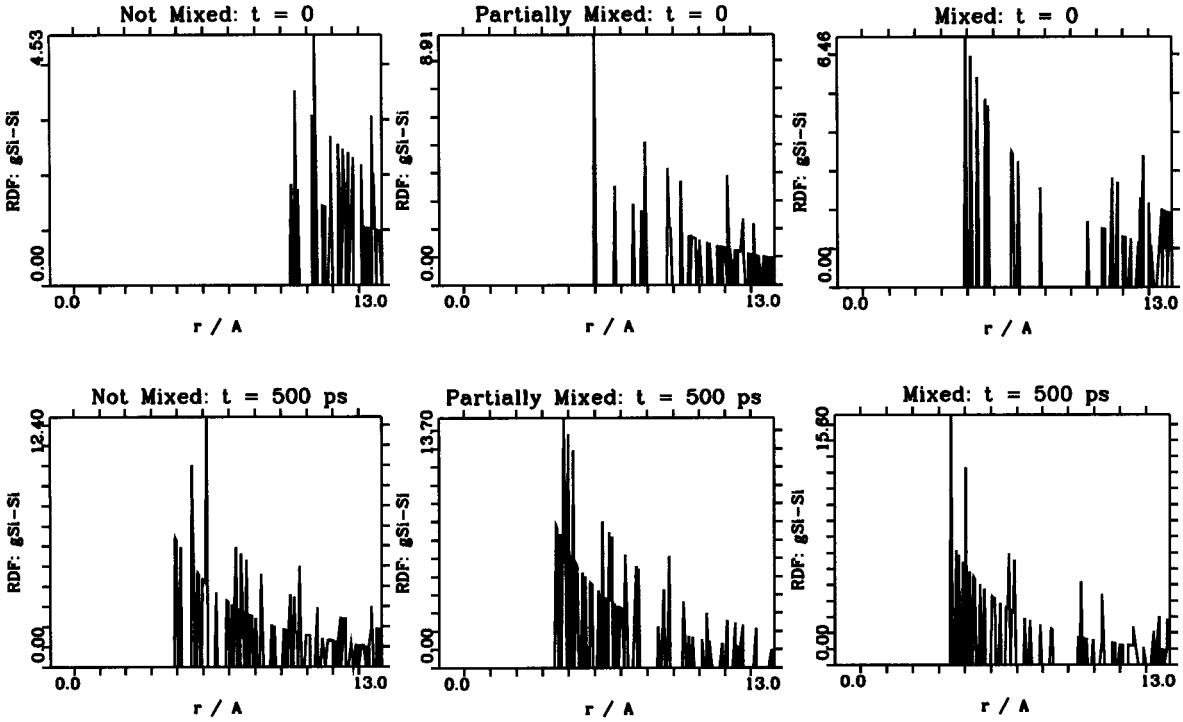

Figure 7. Instantaneous Si−Si pair distributions between trimer rings after DISCOVER simulations, in ethanolic solutions, initially mixed, partially mixed, and unmixed, after 500 ps of run time. The density (g/cm^3) and cell length (Å) are indicated for each solution.

While, for $t = 0$, the radial distribution functions are very different for the mixed, partially mixed, and unmixed solutions, for $t = 500$ ps the RDFs become very similar for the three solutions. Furthermore, while for $t = 0$ the distribution of Si−Si peaks seems to be relatively erratic with groups of peaks separated by gaps, for $t = 500$ ps the peak distribution becomes relatively uniform, showing that a reasonable degree of homogeneity has apparently been achieved in the solutions. For $t = 0$, the distance of the first Si−Si peaks decreases with the degree of mixture for the solutions with rings and increases for the solutions with monomers. These opposite trends, which should be attributed to the lack of equilibration in these solutions, are not observed for $t = 500$ ps. For both methanol- and ethanol-based systems, all solutions thus seem to be reasonably mixed and equilibrated at the end of the simulations. These results might be even more pronounced in more concentrated solutions, as in experimental sol−gel solutions, where the statistical weight of the Si−Si interactions is higher.

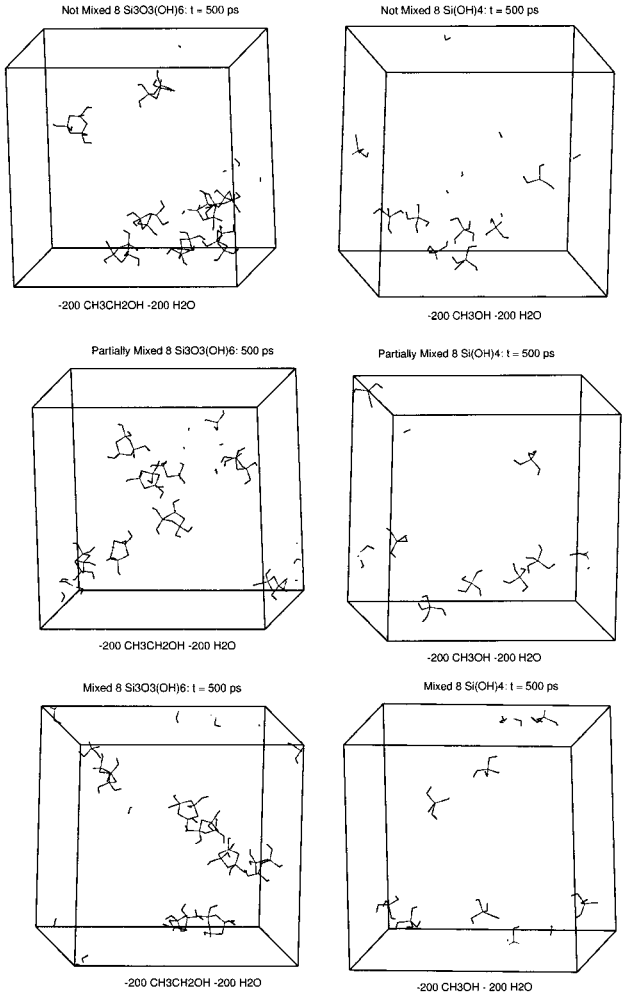

Figure 8. Methanolic and ethanolic solutions after DISCOVER simulations, initially mixed, partially mixed, and unmixed, showing only the silica monomers and trimer rings, after 500 ps of run time.

Surprisingly, the differences between the various solutions cannot be observed in any other RDF interaction, even for $t = 0$. In particular, the radial distribution function between the oxygens in alcohol and water, which might be expected to provide an effective way to follow the progressive mixture of water and alcohol, is almost equal in the three solutions, even for $t = 0$. This happens because, even in the unmixed solutions, there are large water−alcohol interfaces that ensure a significant interaction between the two molecular types.

Density and Energy with DL_POLY. The density and energy contributions for the six sol−gel solutions, collected simultaneously with the radial distribution functions discussed above, are presented in Tables 1 and 2. In all solutions, the density remains constant with time, as the small differences observed are below the uncertainties of the method. The structural changes occurring with time, in all solutions, do not affect their total volume. This behavior is confirmed by the densities of the initial solutions, which match exactly the predicted values for ideal solutions. In particular, water−alcohol contraction effects are not observed. Furthermore, the density also remains unchanged with the progression of the sol−gel process, though a small increase might be noticeable after the hydrolysis in the methanolic solutions. During simulated sol−gel processes, the density increases substantially, but certainly that effect cannot be observed by analyzing only the very beginning of the process, the alkoxide hydrolysis, and the monomer condensation. Additionally, in a real sol−gel experiment, this increase in density is also due to water and alcohol evaporation during the long time needed to reach the gel-point, a mass transfer effect which is not simulated here. The equal densities observed for the various stages of the sol−gel process show also that the charges and zeolite parameters used to describe the monomer and dimer are reasonable, an important test that widely confirms the reliability of the methodology previously developed to simulate liquids by molecular dynamics.

As for the density, the total and partial energies of each solution do not change significantly with the time during the whole MD run. This seems to happen because only a few of the large number of interactions occurring in these solutions are actually changing significantly when aggregation takes place: essentially the Si−Si and Si−O interactions. Thus the decrease in energy becomes smaller than the energy fluctuations. The same happens in the (dilute) DISCOVER solutions, and should be accurately observed only in more concentrated solutions with fewer solvent interactions. The driving forces promoting aggregation must also be considerably weaker in dilute solutions, and the diffusion process should be observed only after relatively long simulation times, as reported here. This essentially "ideal" behavior in energy terms is in line with the ideal behavior in volume discussed above and fully corroborates the identical conclusions obtained for the DISCOVER sol−gel solutions simulated with a Coulombic cutoff, group-based method.

For methanol- and ethanol-based solutions, the total energy decreases considerably from the first to the second solutions (during hydrolysis) and increases from the second to the third solutions (during the condensation). Although these differences are not particularly important in the dynamic and structural studies reported here, as the six sol−gel solutions are independent, they are absolutely critical to developing a realistic MD or MC model of the hydrolysis and condensation reactions. Because these differences in energy are essentially the same in methanolic and ethanolic solutions, they are independent of the alkyl groups in the alkoxide and alcohol. A closer look at the energies presented in Table 2 shows that they originate from the Coulombic contributions. These large differences cannot be due to intermolecular Coulombic interactions, because these are similar in the various solutions. The differences are the result of the intramolecular electrostatic interactions in $Si(OR)_4$, $Si(OH)_4$, and $Si_2O(OH)_6$ (we note that all the charges used to describe these interactions were obtained from ab initio calculations, as discussed in the *Computational Details* section). Because 1−3 and 1−4 interactions are set up to 0.0 and 1.0, respectively, each $Si(OH)_4$ cluster has six strong O−H interactions (hydrogen bonds) compensated only by six much weaker H−H interactions, as the 1−3 O−O interactions are ignored. In $Si_2O(OH)_6$, there are only three O−H and (H−H) short-range interactions per Si atom, and the repulsive 1−5 O−O interactions are already considered. In $Si(OR)_4$, the charges are smaller and the repulsive O−C and Si−H interactions compensate the attractive Si−C and O−H interactions. Because intramolecular Coulombic interactions are so important in $Si(OH)_4$ and $Si_2O(OH)_6$, they distort these molecules and the bond, angle, and dihedral energies increase accordingly, as can be seen in the same table.

Although these intramolecular effects and the corresponding differences in total energy between the various solutions are not particularly important in the dynamic and solvation studies reported here, they are fundamental in describing correctly the energetics of chemical reactions by MD or MC. In particular,

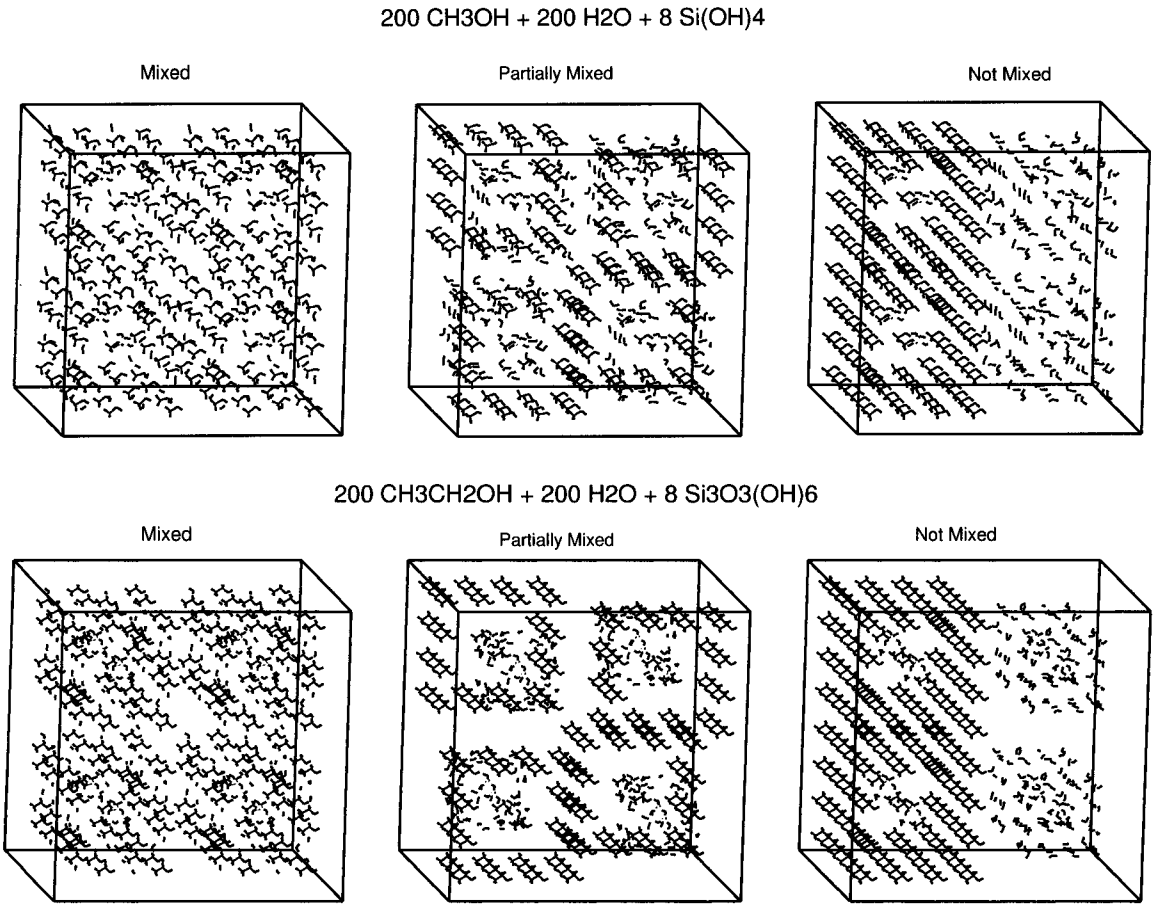

Figure 9. Initial configurations, mixed, partially mixed, and unmixed, in DISCOVER simulations, for methanolic solutions, containing 200 water molecules plus 200 methanol molecules plus 8 monomers $Si(OH)_4$, and ethanolic solutions, containing 200 water molecules plus 200 ethanol molecules plus 8 trimer rings $Si_3O_3(OH)_6$.

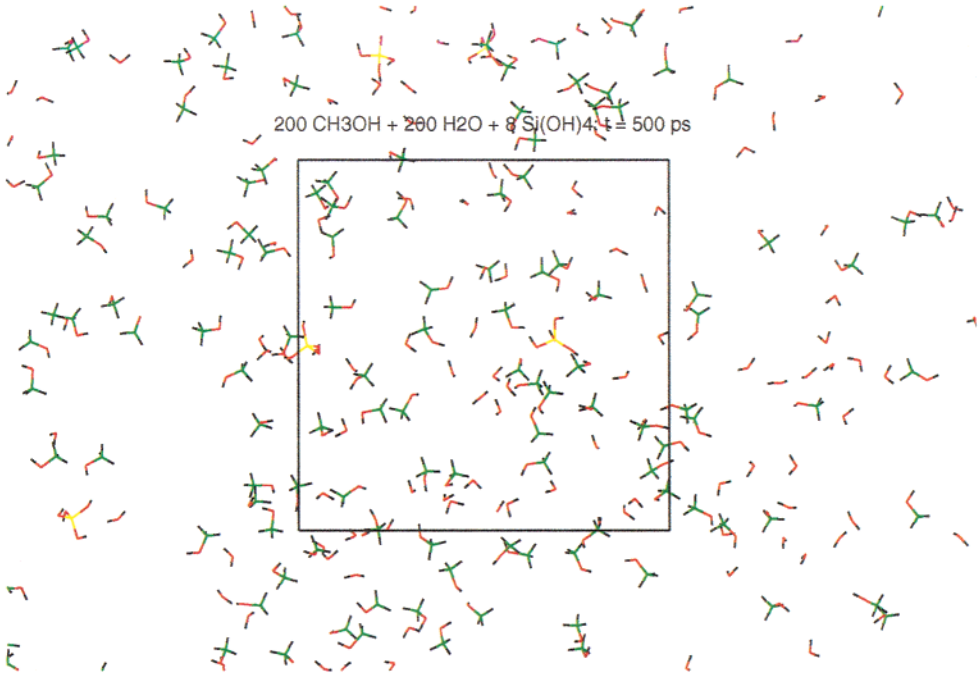

Figure 10. Methanolic solution, initially unmixed, containing 200 water molecules plus 200 methanol molecules plus 8 monomers $Si(OH)_4$, after simulation with DISCOVER, for $t = 500$ ps.

the scaling factors for 1−2, 1−3, 1−4, 1−5, etc. interactions, usually an undervaluated aspect of MD and MC simulations, need to be chosen very carefully to get consistent results for the different chemical arrangements.

Density and Energy with DISCOVER. The mean values of energy, temperature, pressure, and density, for all run times and mixing conditions, are shown in Tables 3 and 4, for the methanolic and ethanolic solutions, respectively. Although the

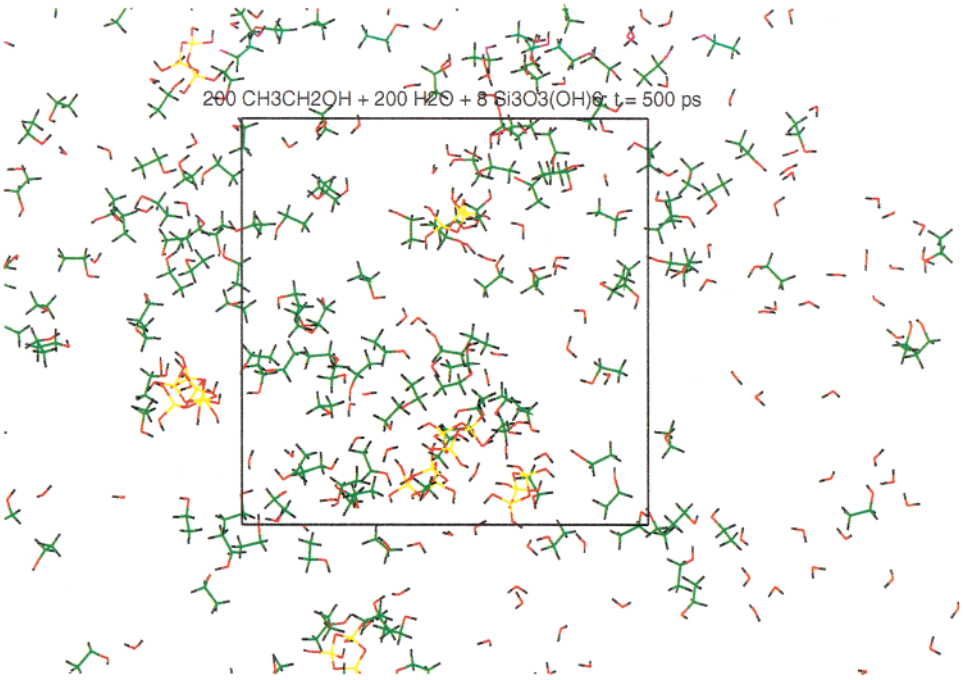

Figure 11. Ethanolic solution, initially unmixed, containing 200 water molecules plus 200 ethanol molecules plus 8 trimer rings $Si_3O_3(OH)_6$, after simulation with DISCOVER, for $t = 500$ ps.

TABLE 1: Calculated and Ideal-Solution Density (gcm^{-3}) for Methanolic and Ethanolic Sol−Gel Solutions after DL_POLY Simulations before Hydrolysis; after Hydrolysis but before Condensation; and after Condensation (all values represent averages over 5 ps)

time/ps	H_2O MeOH $Si(OMe)_4$	MeOH $Si(OH)_4$	H_2O MeOH $Si_2O(OH)_6$	H_2O EtOH $Si(OEt)_4$	EtOH $Si(OH)_4$	H_2O EtOH $Si_2O(OH)_6$
100	0.872	0.879	0.892	0.845	0.848	0.851
300	0.871	0.890	0.880	0.841	0.858	0.851
500	0.869	0.896	0.884	0.860	0.859	0.851
ideal	0.876			0.844		

TABLE 2: Energy (kcal/mol) of Methanolic (Me) and Ethanolic (Et) Sol−Gel Solutions after DL_POLY Simulations before Hydrolysis (b. H.), after Hydrolysis but before Condensation (a. H. b. C.), and after Condensation (a. C.)[a]

soln	time	bond	coul.	VdW	poten.	kinet.	total
Me							
b. H.	100	848.2	7,352.8	−882.2	7,318.8	2,122.5	9,441.3
	300	851.9	7,347.0	−876.1	7,322.7	2,122.5	9,445.2
	500	855.5	7,318.7	−869.2	7,305.0	2,122.5	9,427.5
a. H. b. C	100	8330.7	−44,927	1,467.4	−35,129	2,122.5	−33,006
	300	8397.7	−45,004	1,456.5	−35,150	2,122.5	−33,027
	500	8369.7	−44,998	1,443.2	−35,185	2,122.5	−33,062
a. C.	100	2286.9	−6,619.9	−846.8	−5,179.7	2,122.5	−3,057.2
	300	2271.3	−6,559.4	−846.2	−5,134.3	2,122.5	−3,011.8
	500	2266.4	−6,563.4	−845.2	−5,142.2	2,122.5	−3,019.7
Et							
b. H.	100	428.1	−14,149	−771.7	−14,492	3,066.2	−11,426
	300	431.6	−14,134	−775.3	−14,477	3,066.3	−11,411
	500	451.3	−14,198	−808.8	−14,556	3,066.3	−11,489
a. H. b. C	100	8048.8	−69,654	1,721.5	−59,884	3,066.2	−56,817
	300	8094.1	−69,727	1,698.8	−59,934	3,066.2	−56,867
	500	8064.2	−69,724	1,689.5	−59,971	3,066.2	−56,904
a. C.	100	1974.1	−31,205	−618.6	−29,850	3,066.3	−26,783
	300	1959.3	−31,198	−620.5	−29,859	3,066.3	−26,793
	500	1966.2	−31,235	−616.2	−29,885	3,066.3	−26,814

[a] Bond terms represent bond, angle, and dihedral interactions between bonded atoms. All values represent averages over 5 ps.

potential energy seems to decrease from 0 to 500 ps, particularly for the more bulky ethanolic solutions where equilibration should take more time, no clear trend can be observed. What is more, no visible trends can be found between the results of the mixed, partially mixed, and unmixed solutions: the energy, density, and pressure differences between the various solutions are smaller than the time oscillations observed for these quantities.

Even for the ethanolic solutions, where differences should be more noticeable, the partially mixed solution has the highest energy for $t = 0$, the lowest for $t = 100$ ps, and the highest again for $t = 200$ ps. Definitely, no clear trends can be observed

TABLE 3: Total Energy (kcal/mol), Temperature (°C), Pressure (bar), and Density (gcm^{-3}) as a Function of Time (ps) after DISCOVER Simulations for Mixed (mix), Partially Mixed (par), and Not Mixed (not) Methanol-Based Solutions [200H_2O + 200CH_3OH + 8Si(OH)]

time	soln	E	ΔE	T	ΔT	P	ΔP	ρ	$\Delta\rho$
0	not	350.1	35.6	293.0	1.1	−14.3	191.8	0.830	0.005
	par	329.6	28.6	293.0	1.0	−8.2	173.0	0.850	0.004
	mix	312.6	35.9	293.0	1.0	0.3	193.5	0.848	0.004
100	not	303.5	25.9	293.0	0.9	−4.9	164.0	0.845	0.003
	par	342.6	27.1	293.0	0.9	−17.3	164.7	0.839	0.006
	mix	329.2	25.2	293.0	1.0	5.4	213.5	0.841	0.008
200	not	365.9	29.1	293.0	1.0	−16.2	187.8	0.829	0.004
	par	319.8	38.2	293.0	1.0	−21.2	196.7	0.843	0.006
	mix	309.4	29.0	293.0	0.9	−12.4	177.4	0.845	0.005
300	not	326.2	35.7	293.0	1.0	−12.5	175.9	0.844	0.005
	par	362.5	31.2	293.0	1.0	−22.1	196.5	0.832	0.004
	mix	329.7	26.7	293.0	1.0	10.9	187.6	0.846	0.010
400	not	345.4	42.2	293.0	1.0	−8.2	187.8	0.832	0.008
	par	311.5	30.9	293.0	1.0	19.5	169.8	0.846	0.006
	mix	328.8	31.1	293.0	1.1	−16.1	178.2	0.835	0.006
500	not	333.8	34.0	293.0	1.0	−10.1	160.4	0.837	0.008
	par	307.1	36.9	293.0	1.0	−9.5	177.5	0.848	0.005
	mix	342.7	30.0	293.0	1.0	−34.4	181.6	0.837	0.008

TABLE 4: Total Energy (kcal/mol), Temperature (°C), Pressure (bar), and Density (gcm^{-3}) as a Function of Time (ps) after DISCOVER Simulations for Mixed (mix), Partially Mixed (par), and Not Mixed (not) Ethanolic Solutions [200H_2O + 200CH_3CH_2OH + 8$Si_3O_3(OH)_6$]

time	soln	E	ΔE	T	ΔT	P	ΔP	ρ	$\Delta\rho$
0	not	−10,017.7	38.0	293.0	0.9	−23.9	232.5	0.846	0.007
	par	−9,994.3	28.8	293.0	0.9	−2.7	190.7	0.840	0.006
	mix	−10,013.0	30.2	293.0	0.9	6.1	191.9	0.848	0.005
100	not	−10,015.5	33.3	293.0	0.9	10.5	192.3	0.852	0.003
	par	−10,045.9	31.3	293.0	0.9	−8.5	161.2	0.856	0.004
	mix	−10,020.1	35.7	293.0	0.9	−25.1	205.0	0.842	0.006
200	not	−10,028.7	36.1	293.0	0.9	3.5	169.8	0.851	0.004
	par	−10,001.7	43.8	293.0	0.9	−0.8	190.3	0.846	0.006
	mix	−10,034.5	32.6	293.0	0.9	−6.1	185.5	0.858	0.005
300	not	−9,999.6	50.0	293.0	0.9	7.0	215.3	0.850	0.004
	par	−9,981.7	33.8	293.0	0.8	−3.1	186.7	0.832	0.004
	mix	−10,017.9	37.0	293.0	0.9	5.0	176.6	0.847	0.003
400	not	−10,020.8	35.5	293.0	0.8	−14.2	170.4	0.841	0.004
	par	−10,037.7	38.3	293.0	0.9	−2.6	169.2	0.859	0.004
	mix	−10,053.1	32.0	293.0	0.8	3.8	168.5	0.859	0.004
500	not	10,042.9	34.8	293.0	0.9	−1.2	193.3	0.856	0.006
	par	−10,045.8	34.9	293.0	0.9	−20.0	197.3	0.848	0.006
	mix	−10,077.0	36.2	293.0	0.9	−5.1	171.3	0.862	0.005

for different solutions or times after the short initial period of compression (10 ps) and relaxation (20 ps) to ambient conditions, which is surprising, because the visual inspection of the solutions and the analysis of the Si−Si RDFs show that significant differences between the various solutions still persist after 200−300 ps.

Short Data Collection Times with DL_POLY. The density and energy results discussed so far were obtained after run times of 100, 300 and 500 ps and a collecting time of 5 ps. Equivalent results covering every 50 ps of run time, with a collection time of 0.5 ps, are presented in Tables 5 and 6. As before, no differences in density and energy are observed during the whole range of times analyzed. The density and total energy for t = 100, 300, and 500 ps are also similar (for all six solutions) to the values presented above, with collecting times that are 10 times larger. This shows that, for properly equilibrated solutions, sampling times as small as 0.5 ps can produce reliable results, even if the signal/noise ratio is poor.

Short Run Times with DL_POLY. The results discussed so far have been obtained after long MD run times. The density

TABLE 5: Density (gcm^{-3}) as a Function of Time (ps) for Methanolic and Ethanolic Solutions after DL_POLY Simulations before Hydrolysis, after Hydrolysis but before Condensation, and after Condensation (all values represent averages over 1 ps)

time/ps	H_2O MeOH $Si(OMe)_4$	MeOH $Si(OH)_4$	H_2O MeOH $Si_2O(OH)_6$	H_2O EtOH $Si(OEt)_4$	EtOH $Si(OH)_4$	H_2O EtOH $Si_2O(OH)_6$
100	0.861	0.886	0.895	0.853	0.851	0.850
150	0.885	0.899	0.884	0.865	0.852	0.853
200	0.887	0.873	0.881	0.849	0.851	0.851
250	0.874	0.888	0.884	0.845	0.848	0.857
300	0.875	0.892	0.882	0.843	0.857	0.854
350	0.885	0.882	0.895	0.849	0.856	0.844
400	0.876	0.898	0.893	0.853	0.852	0.854
450	0.871	0.892	0.883	0.845	0.849	0.857
500	0.859	0.896	0.874	0.858	0.861	0.857

TABLE 6: Total Energy (kcal/mol), as a Function of Time, for Methanolic and Ethanolic Solutions after DL_POLY Simulations before Hydrolysis, after Hydrolysis but before Condensation, and after Condensation (all values represent averages over 1 ps)

time/ps	H_2O MeOH $Si(OMe)_4$	MeOH $Si(OH)_4$	H_2O MeOH $Si_2O(OH)_6$	H_2O EtOH $Si(OEt)_4$	EtOH $Si(OH)_4$	H_2O EtOH $Si_2O(OH)_6$
100	9,446.9	−33,039	−3,075.2	−11,458	−56,836	−26,773
150	9,386.1	−33,026	−3,020.7	−11,497	−56,882	−26,801
200	9,391.8	−32,978	−3,019.4	−11,438	−56,800	−26,826
250	9,445.4	−33,028	−3,050.2	−11,442	−56,834	−26,832
300	9,460.2	−32,992	−3,008.7	−11,431	−56,804	−26,812
350	9,393.9	−33,007	−3,038.8	−11,432	−56,794	−26,787
400	9,433.8	−33,084	−3,033.6	−11,454	−56,889	−26,812
450	9,430.0	−33,073	−2,986.8	−11,437	−56,894	−26,826
500	9,440.0	−33,066	−3,029.4	−11,488	−56,916	−26,831

and total energy in the beginning of the simulations, for t = 0, 5 and 10 ps (20 000 time steps) are presented in Table 7. A comparison with the results of the Tables 5 and 6 shows that for short run times the densities tend to be slightly lower (and the energies slightly higher) than in the fully equilibrated solutions, but the differences are usually small, in some cases below the uncertainty of the method. Consequently, the results reported in our previous article[1] for the pure liquids, after 22.5 ps of equilibration time and 2.5 ps of collection time, should remain almost unaltered after arbitrarily long run times or better data sampling.

Solvation Effects with DL_POLY. Figures 12, 13, and 14 show the solvation environment around chosen silica clusters, observed at the end of the simulations, for the three types of ideal solutions studied here: before hydrolysis; after hydrolysis and before condensation; and after the first stage of condensation. To diversify the analysis, the first image was taken from the methanolic solution, while the other two came from the ethanolic solutions. Because these solutions emulate real sol−gel solutions with compositions commonly used in experimental work, the images should be realistic representations of the liquid structure around the reactant clusters, therefore providing a valuable tool for studying the chemistry of the reactions and for developing realistic potentials to simulate them, using purely classic techniques. Although these instantaneous local images do not pretend to represent average or even typical environments for the various silica clusters (we chose the environments where more silica clusters surrounded the central cluster, to emphasize the agreggation effects), some preliminary conclusions can be drawn.

In all cases, the first solvation layer seems to be formed by 5−8 molecules, forming hydrogen bonds with the central cluster at distances between 1.75 and 2.5 Å. The number of molecules

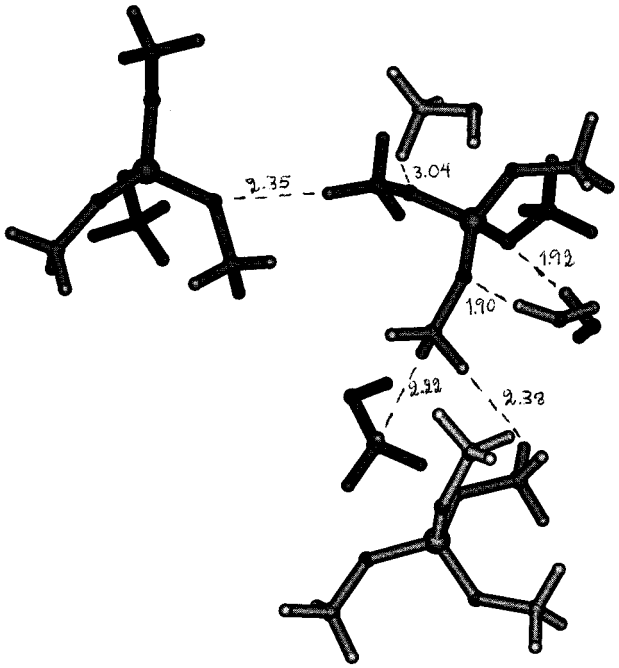

Figure 12. Solvation environment around an alkoxide, in a methanolic solution before hydrolysis, after DL_POLY simulation, showing all clusters at a distance smaller than 2.5 Å.

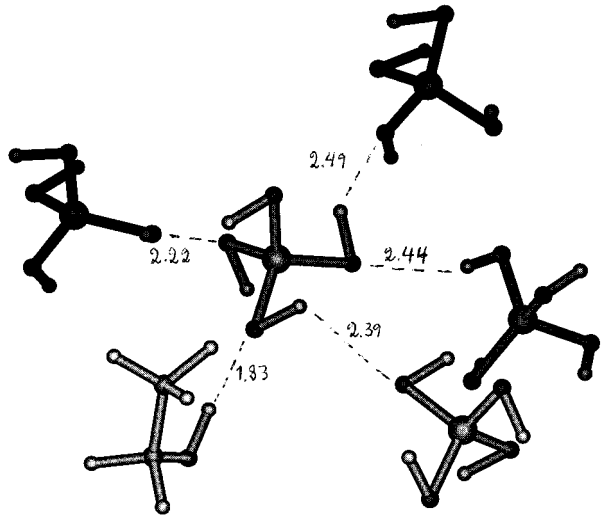

Figure 13. Solvation environment around a monomer, in an ethanolic solution between hydrolysis and condensation, after DL_POLY simulation, showing all clusters at a distance smaller than 2.5 Å.

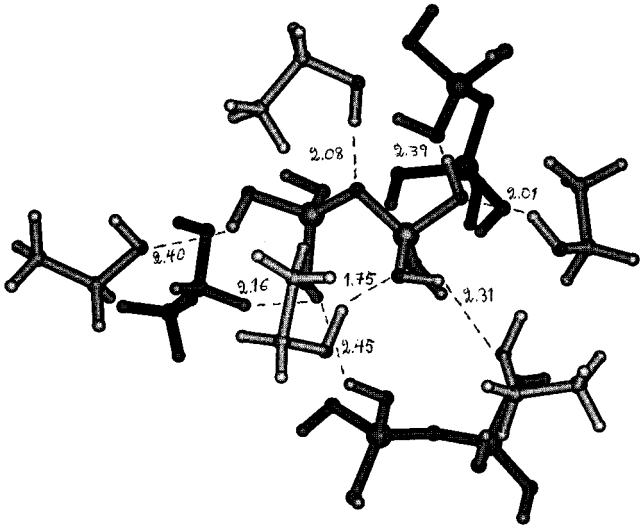

Figure 14. Solvation environment around a dimer, in a ethanolic solution after condensation, after DL_POLY simulation, showing all clusters at a distance smaller than 2.5 Å.

surrounding each cluster will increase for bigger clusters, but the number of neighbors per contact area is likely to change little, for clusters of the same type (this contact area is larger for uncyclic clusters than for rings). The importance of the hydrogen bonds in the sol−gel liquid structure is clearly evidenced in these images, and in fact they are likely to represent the main competition for the O−Si interactions that need to take place for the forward reactions to occur. As the key O−Si interactions for the forward and reverse sol−gel reactions were discussed in detail previously, we concentrate here on the closer O−H interactions.

Figure 12 shows two water molecules separated only by 1.9 Å of the oxygen atoms in the central silica alkoxide, an indication that water molecules can easily diffuse to the central $Si(O)_4$ region of the silica alkoxides, a required step for the hydrolysis replacement of a Si−OR bond by a Si−OH bond to take place. Although some alcohol molecules can also be seen in this first solvation layer, they appear at larger distances than the water molecules.

What is more important in the solvation environment shown in Figure 13 is the substantial number of silica monomers surrounding the central monomer, nothing less than four, forming weak hydrogen bonds with the central cluster at distances varying from 2.22 to 2.49 Å. By contrast, only one alcohol molecule is in the first solvation layer shown in the image—rather impressive considering that this solution contained 360 molecules of alcohol and only 30 silica monomers. This shows that the probability of a cluster interacting directly with another cluster in a realistic sol−gel solution is high, clearing the way for the condensation reactions and silica growth in solution. In particular, this solvation arrangement suggests that small rings might be formed directly from aggregated monomers.

Figure 14 shows a dimer surrounded by two dimers and six alcohol molecules. Although water molecules are present in this

TABLE 7: Density (gcm^{-3}) and Total Energy (kcal/mol) after a Short Run Time (ps) for Methanolic and Ethanolic Solutions after DL_POLY Simulations before Hydrolysis, after Hydrolysis but before Condensation, and after Condensation (all values represent averages over 1 ps)

time/ps	H_2O MeOH $Si(OMe)_4$	MeOH $Si(OH)_4$	H_2O MeOH $Si_2O(OH)_6$	H_2O EtOH $Si(OEt)_4$	EtOH $Si(OH)_4$	H_2O EtOH $Si_2O(OH)_6$
0	0.845	0.866	0.872	0.844	0.848	0.848
	9,523.5	−32,788	−2,901.2	−11,419	−56,599	−26,781
5	0.854	0.862	0.864	0.844	0.850	0.848
	9,522.6	−32,782	−2,927.6	−11,408	−56,623	−26,783
10	0.869	0.875	0.862	0.843	0.851	0.842
	9,477.7	−32,816	−2,980.1	−11,409	−56,599	−26,763

solution, none appears in this image due to their small number (only 15). The aggregation of the dimers is again very significant, considering that there are only 15 dimers for 240 alcohol molecules in this solution. The hydrogen bonds formed between the alcohol molecules and the dimers are stronger that those formed between the dimers, suggesting that the reverse reesterification (replacing SiOH by SiOR bonds) may have a significant role in the global sol−gel process.

Important deviations from the equilibrium intramolecular configurations can be observed for all systems shown here, as these images act as instantaneous snapshots of the system, freezing the molecular vibrations. To understand the dynamic mechanisms that ultimately lead to the sol−gel chemical reactions, which are determined not only by the electronic distribution but also by the vibrational framework in these systems, it will be important to extend this method to produce dynamic images of the evolution of the solutions. A detailed quantitative analysis of the structure in the bulk of these liquid systems, as a function of time, will prove fundamental to develop potentials and methodologies to simulate these reaction processes using molecular dynamics or Monte Carlo techniques.

Conclusions

The MD simulations presented here have aimed to provide a realistic description of sol−gel solutions, following our earlier work on pure liquids. Currently, the mechanisms of chemical reactions cannot be modeled in these purely classical simulations, so ideal solutions representing stages of the sol−gel process have to be considered. The results obtained help to clarify three important problems related to diffusion in liquid solutions: aggregation, mixture, and solvation.

The results obtained for all solutions simulated with DL_POLY show that silica clusters tend to aggregate after a relatively long time. Furthermore, the mechanism of diffusion favors always the intermolecular interactions leading to the forward reactions, which become systematically more important, for long run times, than the interactions leading to the reverse reactions. This aggregation effect is confirmed entirely by the results obtained for all solutions simulated with DISCOVER, with a key O−Si intermolecular distance that can be smaller than 3 Å. In both DL_POLY and DISCOVER solutions, the aggregation seems to be more pronounced between larger silica clusters. These results are essential in constructing a theoretical model able to perform realistic simulations of silica-based sol−gel processes. The fact that these aggregation effects have been observed with two different MD methods, implemented in two different codes for many different dilute solutions containing various different silica clusters, gives confidence in the general conclusions drawn from the simulations.

Another important result is that the progressive equilibration of a solution formed by initially unmixed species is effectively described by an MD simulation, occurring in a time short enough to be followed by this method. This behavior is observed even in the most difficult conditions, with initial configurations that are very far from equilibrium and with relatively large molecules, for which the diffusion is slow. This guarantees that the initial configuration is not critical in obtaining accurate results in the simulation of very complex solutions.

Despite these structural changes, no significant variations with time are observed for the density and energy in both DL_POLY and DISCOVER solutions, a somewhat surprising result that seems to be due to the small number of interactions that are actually affected by such changes in these dilute solutions. In particular, the total energy, density, and even RDFs of DISCOVER solutions with different degrees of initial mixing become essentially equal (within the uncertainty of the method) after relatively short MD run times.

The simulation of sol−gel solutions, with compositions used in experimental work, provides also a useful tool for studying the solvation environment of the silica clusters in solution, by direct observation of the atomic arrangements around each cluster. In particular, this analysis will prove invaluable in the development of potentials to simulate accurately the competing mechanisms of reaction and solvation that take place in sol−gel solutions. The successful completion of these simulations will provide a firm basis for understanding and controlling these important and exciting systems.

Acknowledgment. We are grateful to EPSRC for funding the local and national computer facilities used for this work. We are grateful to MSI for the provision of the DISCOVER code and other software. One of the authors (J.C.G.P.) is greatly indebted to JNICT, Lisboa, Project Praxis XXI/CTM/12041/98, for their financial support.

Appendix: Force Field

We now describe the force field used in all DL_POLY and DISCOVER simulations reported in this work, including atomic charges, bonding and van der Waals potentials (Tables 8−12). Cross terms are not included due to lack of space and because they were used in DISCOVER but not in DL_POLY simulations, slightly more accurate.

TABLE 8: Hirshfeld Ab-initio Charges, Multiplied by 2.7, Used in DL_POLY Simulations[a]

H_2O	ohh: −0.8170	ho: 0.4085
CH_3OH	c3: −0.1820	h3:0.1183
	o: −0.5943	ho: 0.4214
CH_3CH_2OH	c3: −0.3660	h3: 0.1323
	c2: −0.0626	h2: 0.0956
	o: −0.5783	ho: 0.4188
$Si(OCH_3)_4$	sz4: 1.2540	osc: −0.5535
	c3: −0.1479	h3: 0.1293
$Si(OCH_2CH_3)_4$	sz4: 1.2452	osc: −0.5416
	c3: −0.3610	h3: 0.1342
	c2: −0.0311	h2: 0.1099
$Si(OH)_4$	osh: −0.7673	hos: 0.4655
	sz0: 1.2072	
$Si_2O(OH)_6$	osh: −0.7266	hos: 0.4377
	sz1: 1.2415	oss: −0.7496
$Si_3O_3(OH)_6$	oss: −0.7366	sz2: 1.2722
	osh: −0.7468	hos: 0.4790

[a] In DISCOVER simulations, Hirshfeld charges were multiplied by 2.6.

TABLE 9: Quartic Bond Potentials Used in Both DL_POLY and DISCOVER Simulations to Calculate Bond Energy: energy(kcal/mol) = $K_2(r - r_0)^2 + K_3(r - r_0)^3 + K_4(r - r_0)^4$

atom type *i*	atom type *j*	r_0 (Å)	K_2	K_3	K_4
c	hc	1.1010	341.0000	−691.8900	844.6000
c	c	1.5330	299.6700	−501.7700	679.8100
c	o	1.4200	400.3954	−835.1951	1313.0142
ho	o	0.9650	532.5062	−1282.9050	2004.7658
ho	ohh	0.9700	563.2800	−1428.2200	1902.1200
sz	oss	1.6097	414.3500	−1252.1779	1179.6300
sz	osh	1.6128	442.6452	−791.5413	0.0000
osh	hos	0.9464	694.8248	−1548.1306	2883.4712
c	osc	1.4200	400.3954	−835.1951	1313.0142
sz	osc	1.6097	414.3500	−1252.1779	1179.6300

TABLE 10: Quartic Angle Potentials Used in Both DL_POLY and DISCOVER Simulations to Calculate Angle Energy: energy(kcal/mol) = $K_2(\theta - \theta_0)^2 + K_3(\theta - \theta_0)^3 + K_4(\theta - \theta_0)^4$

atom type *i*	atom type *j*	atom type *k*	θ_0 (deg.)	K_2	K_3	K_4
hc	c	hc	107.6600	39.6410	−12.9210	−2.4318
c	c	hc	110.7700	41.4530	−10.6040	5.1290
c	c	c	112.6700	39.5160	−7.4430	−9.5583
c	o	c	104.5000	35.7454	−10.0067	−6.2729
hc	c	o	108.7280	58.5446	−10.8088	−12.4006
c	c	o	111.2700	54.5381	−8.3642	−13.0838
c	o	ho	105.8000	52.7061	−12.1090	−9.8681
ho	ohh	ho	103.7000	49.8400	−11.6000	−8.0000
oss	sz	osh	111.0860	96.8686	−20.3823	78.8805
osh	sz	osh	116.2621	53.8454	33.8899	82.6287
oss	sz	oss	110.9263	134.4324	−34.4450	0.0000
sz	oss	sz	174.2152	4.6647	0.0000	0.0000
sz	osh	hos	118.0442	24.2581	−27.3276	21.0670
sz	osc	c	118.9150	20.2051	−5.0034	−3.1365
osc	sz	oss	110.9263	134.4324	−34.4450	0.0000
osc	sz	osh	111.0860	96.8686	−20.3823	78.8805
osc	sz	osc	108.6038	134.4324	−34.4450	0.0000
osc	c	hc	109.7219	58.5446	−10.8088	−12.4006
osc	c	c	109.5200	54.5381	−8.3642	−13.0838

TABLE 11: Three-Term Torsion Potentials Used in Both DL_POLY and DISCOVER Simulations to Calculate Torsion Energy: energy(kcal/mol) = $\sum_{n=1}^{3} V_n[1 + \cos(n\phi - \phi_n)]$

atom type *i*	atom type *j*	atom type *k*	atom type l	V_1	ϕ_1 (deg)	V_2	ϕ_2 (deg)	V_3	ϕ_3 (deg)
hc	c	c	hc	−0.2432	0.0	0.0617	0.0	−0.1383	0.0
c	c	c	hc	0.0000	0.0	0.0316	0.0	−0.1781	0.0
c	c	c	c	0.1223	0.0	0.0514	0.0	−0.2230	0.0
hc	c	o	c	0.5302	0.0	0.0000	0.0	−0.2836	0.0
c	c	o	c	−0.5203	0.0	−0.3028	0.0	−0.3450	0.0
hc	c	c	o	−0.1435	0.0	0.2530	0.0	−0.0905	0.0
c	c	c	o	0.7137	0.0	0.2660	0.0	−0.2545	0.0
o	c	c	o	−0.1820	0.0	−0.1084	0.0	−0.7047	0.0
hc	c	o	ho	0.1863	0.0	−0.4338	0.0	−0.2121	0.0
c	c	o	ho	−0.6732	0.0	−0.4778	0.0	−0.1670	0.0
osh	sz	oss	sz	−0.9570	0.0	0.0758	0.0	0.0000	0.0
oss	sz	osh	hos	3.9302	0.0	0.3068	0.0	−0.5910	0.0
osh	sz	osh	hos	2.5590	0.0	0.4330	0.0	0.1236	0.0
oss	sz	oss	sz	−0.9614	0.0	0.0000	0.0	0.0000	0.0
osc	sz	oss	sz	−0.9614	0.0	0.0000	0.0	0.0000	0.0
osc	sz	osh	hos	3.9302	0.0	0.3068	0.0	−0.5910	0.0
osc	sz	osc	c	−0.9614	0.0	0.0000	0.0	0.0000	0.0
oss	sz	osc	c	−0.9614	0.0	0.0000	0.0	0.0000	0.0
osh	sz	osc	c	−0.9570	0.0	0.0758	0.0	0.0000	0.0
sz	osc	c	c	−0.5203	0.0	−0.3028	0.0	−0.3450	0.0
sz	osc	c	hc	0.5302	0.0	0.0000	0.0	−0.2836	0.0
osc	c	c	hc	−0.1435	0.0	0.2530	0.0	−0.0905	0.0

TABLE 12: Parameters Used in Both DL_POLY and DISCOVER Simulations to Describe van der Waals 9−6 Interactions[a]

atom type	σ (Å)	ϵ (kcal/mol)
c	4.0100	0.0540
o	3.5350	0.2400
ohh	3.6080	0.2740
hc	2.9950	0.0200
ho	1.0980	0.0130
sz0	4.4350	0.0950
sz1	4.4350	0.0950
sz2	4.4350	0.0950
oss	3.4506	0.1622
osh	3.4618	0.1591
hos	2.3541	0.0988
osc	3.5350	0.2400

[a] Combined parameters and energy are obtained according to the equations $\sigma_{ij} = (\sigma_i^6 + \sigma_j^6/2)^{1/6}$; $\epsilon_{ij} = 2\sqrt{\epsilon_i\epsilon_j}\sigma_i^3\sigma_j^3/(\sigma_i^6 + \sigma_j^6)$; energy-(kcal/mol) = $\epsilon_{ij}[2(\sigma_{ij}/r_{ij})^9 - 3(\sigma_{ij}/r_{ij})^6]$.

References and Notes

(1) Pereira, J. C. G.; Catlow, C. R. A.; Price, G. D. *J. Phys. Chem. A* **2001**, *105*, 1909.

(2) Pereira, J. C. G.; Catlow, C. R. A.; Price G. D. *J. Phys. Chem. A* **1999**, *103*, 3252.

(3) Pereira, J. C. G.; Catlow, C. R. A.; Price G. D. *J. Phys. Chem. A* **1999**, *103*, 3268.

(4) Livage, J.; Sanchez, C. *J. Non-Cryst. Solids* **1992**, *145*, 11.

(5) Brinker, C. J.; Scherer, G. W. *The Physics and Chemistry of Sol−Gel Processing*; Academic Press: New York, 1989.

(6) Uhlmann, D. R.; Zelinski, B. J.; Silverman, L.; Warner, S. B.; Fabes, B. D.; Doyle, W. F. In *Science of Ceramic Chemical Processing*; Hench, L. L., Ulrich, D. R., Eds.; John Wiley & Sons: New York, 1986; Chapter 19, p 173.

(7) Iler, R. K. *The Chemistry of Silica*; John Wiley & Sons: New York, 1979.

(8) Osterholtz, F. D.; Pohl, E. R. *J. Adhes. Sci. Technol.* **1992**, *6−1*, 127.

(9) Mackenzie, J. D. In *Science of Ceramic Chemical Processing*; Hench L. L., Ulrich, D. R., Eds.; John Wiley & Sons: New York, 1986; p 113.

(10) Jonas, J. In *Science of Ceramic Chemical Processing*; Hench L. L., Ulrich, D. R., Eds.; John Wiley & Sons: New York, 1986; p 65.
(11) Jonas, J. In *Ultrastructure Processing of Advanced Materials*; Uhlmann, D. R., Ulrich, D. R., Eds.; John Wiley & Sons: New York, 1992; p 13.
(12) Orcel, G.; Hench, L. L. *J. Non-Cryst. Solids* **1986**, *79*, 177.
(13) Orcel, G.; Hench, L. L.; Artaki, I.; Jonas, J.; Zerda, T. W. *J. Non-Cryst. Solids* **1988**, *105*, 223.
(14) Artaki, I.; Bradley, M.; Zerda, T. W.; Jonas, T. W.; Orcel, G.; Hench, L. L. In *Science of Ceramic Chemical Processing*; Hench L. L., Ulrich, D. R., Eds.; John Wiley & Sons: New York, 1986; p 73.
(15) Peppas, N. A.; Scranton, A. B.; Tsou, A. H.; Edwards, D. E. In *Better Ceramics Through Chemistry III*; Materials Research Society series; Brinker, C. J., Clark, D. E., Ulrich, D. R., Eds.; Elsevier Science Publishing Co.: New York, 1988; 121, 43.
(16) Assink, R. A.; Kay B. D. *J. Non-Cryst. Solids* **1988**, *99*, 359.
(17) Re, N. *J. Non-Cryst. Solids* **1992**, *142*, 1.
(18) Kay, B. D.; Assink, R. A. *J. Non-Cryst. Solids* **1988**, *104*, 112.
(19) Kelts, L. W.; Amstrong, N. J. *J. Mater. Res.* **1989**, *4*−*2*, 423.
(20) Klemperer, W. G.; Mainz, V. V.; Millar, D. M. In *Better Ceramics Through Chemistry II*; Materials Research Society series; Brinker, C. J., Clark, D. E., Ulrich, D. R., Eds.; Elsevier Science Publishing Co.: New York, 1986; 73, 3.
(21) Klemperer, W. G.; Mainz, V. V.; Millar, D. M. In *Better Ceramics Through Chemistry II*; Materials Research Society series; Brinker, C. J., Clark, D. E., Ulrich, D. R., Eds.; Elsevier Science Publishing Co.: New York, 1986; 73, 15.
(22) Klemperer, W. G.; Ramamurthi, S. D. In *Better Ceramics Through Chemistry III*; Materials Research Society series; Brinker, C. J., Clark, D. E., Ulrich, D. R., Eds.; Elsevier Science Publishing Co.: New York, 1988; 121, 1.
(23) Klemperer, W. G.; Ramamurthi, S. D. In *Better Ceramics Through Chemistry III*; Materials Research Society series; Brinker, C. J., Clark, D. E., Ulrich, D. R., Eds.; Elsevier Science Publishing Co.: New York, 1988; 121, 15.
(24) Klemperer, W. G.; Ramamurthi, S. D. *J. Non-Cryst. Solids* **1990**, *121*, 16.
(25) Knight, C. T. G. *Zeolites* **1990**, *10*, February, 140.
(26) Garofalini, S. H.; Melman H. In *Better Ceramics Through Chemistry II*; Materials Research Society series; Brinker, C. J., Clark, D. E., Ulrich, D. R., Eds.; Elsevier Science Publishing Co.: New York, 1986; 73, 497.
(27) Garofalini, S. H. In *Sol*−*Gel Technology For Thin Films, Fibers, Preforms, Electronics, and Specialty Shapes*; Materials Science and Process Technology series; Klein, L. C., Ed.; Noyes Publications: New Jersey, 1988; p 16.
(28) Feuston, B. P.; Garofalini, S. H. *J. Chem. Phys.* **1990**, *94*, 5351.
(29) Feuston B. P.; Garofalini S. H. *Chem. Phys. Lett.* **1990**, *170*, 264.
(30) Feuston, B. P.; Garofalini, S. H. *J. Chem. Phys.* **1988**, *89*−*9*, 5818.
(31) Garofalini, S. H.; Martin, G. E. *J. Phys. Chem.* **1994**, *98*, 1311.
(32) Martin, G. E.; Garofalini, S. H. *J. Non-Cryst. Solids* **1994**, *171*, 68.
(33) Pohl, P. I.; Faulon, J. L.; Smith, D. M. *J. Non-Cryst. Solids* **1995**, *186*, 349.
(34) Soules, T. S. *J. Non-Cryst. Solids* **1982**, *49*, 29.
(35) Vessal, B.; Leslie M.; Catlow, C. R. A. *Molecular Simulation* **1989**, *3*, 123.
(36) Newell, R. G.; Feustoni, B. P.; Garofalini, S. H. *J. Mater. Res.* **1989**, *4*−*2*, 434.
(37) Zirl, D. M.; Garofalini, S. H. *J. Am. Ceram. Soc.* **1990**, *73*−*10*, 2848.
(38) Melman H.; Garofalini, S. H. *J. Non-Cryst. Solids* **1991**, *134*, 107.
(39) Lasaga, A. C.; Gibbs, G. V. *Phys. Chem. Minerals* **1987**, *14*, 107.
(40) Lasaga, A. C.; Gibbs, G. V. *Phys. Chem. Minerals* **1988**, *16*, 29.
(41) Sauer, J. *Chem. Rev.* **1989**, *89*, 199.
(42) Ahlrichs, R.; Bär, M.; Häser, M.; Kölmel, C.; Sauer, J. *Chem. Phys. Lett.* **1989**, *164*, 199.
(43) Ferrari, A. M.; Ugliengo, P.; Garrone, E. *J. Chem. Phys.* **1993**, *97*, 2671.
(44) Pápai, I.; Goursot, A.; Fajula, F. *J. Chem. Phys.* **1994**, *98*, 4654.
(45) Hill, J.; Sauer, J. *J. Phys. Chem.* **1994**, *98*, 1238.
(46) Moravetski, V.; Hill J.; Eichler, U.; Cheetham, A. K.; Sauer, J. *J. Am. Chem. Soc.* **1996**, *118*, 13015.
(47) Chelikowsky, J. R.; King, H. E., Jr.; Glinnemann, J. *Phys. Rev. B* **1990**, *41*−*15*, 10866.
(48) Kubicki, J. D.; Lasaga, A. C. *Am. Mineral.* **1988**, *73*, 941.
(49) Dereli, G. *Mol. Simul.* **1992**, *8*, 351.
(50) Fleischman, S. H.; Brooks, C. L., III. *J. Chem. Phys.* **1987**, *87*−*5*, 3029.
(51) Stouten, P. F. W.; Kroon, J. *Mol. Simul.* **1990**, *5*, 175.
(52) Howell, P. L.; Goodfellow J. M. *Mol. Simul.* **1988**, *1*, 333.
(53) Yoldas, B. E. *J. Non-Cryst. Solids* **1986**, *82*, 11.
(54) *Discover 96.0 manual*; Molecular Simulations Inc., San Diego CA, 1996.
(55) *DL_POLY manual*; S. E. R. C. Daresbury Laboratory, Daresbury, Warrington WA4 4AD, Cheshire, U.K., 1996.
(56) Allen, M. P.; Tildesley, D. J. *Computer Simulation of Liquids*; Oxford Science Publications: Oxford, 1987.
(57) Pereira, J. C. G.; Catlow, C. R. A.; Price, G. D. *Chem. Commun.* **1998**, 1387.